renuka b

thesis

gdt

Document Details

Submission ID
trn:oid:::3618:140679551

Submission Date
May 27, 2026, 8:54 PM GMT+5:30

Download Date
May 27, 2026, 9:04 PM GMT+5:30

File Name
thesis.docx

File Size
6.9 MB

54 Pages

8,461 Words

52,892 Characters

9% Overall Similarity

The combined total of all matches, including overlapping sources, for each database.

Filtered from the Report

- Bibliography
- Small Matches (less than 10 words)

Exclusions

- 6 Excluded Matches

Match Groups

54 Not Cited or Quoted 9%
Matches with neither in-text citation nor quotation marks

1 Missing Quotations 0%
Matches that are still very similar to source material

0 Missing Citation 0%
Matches that have quotation marks, but no in-text citation

0 Cited and Quoted 0%
Matches with in-text citation present, but no quotation marks

Top Sources

7% Internet sources
5% Publications
6% Submitted works (Student Papers)

Integrity Flags

0 Integrity Flags for Review

Our system's algorithms look deeply at a document for any inconsistencies that would set it apart from a normal submission. If we notice something strange, we flag it for you to review.

A Flag is not necessarily an indicator of a problem. However, we'd recommend you focus your attention there for further review.

Match Groups

- **54** Not Cited or Quoted 9%
  Matches with neither in-text citation nor quotation marks
- **1** Missing Quotations 0%
  Matches that are still very similar to source material
- **0** Missing Citation 0%
  Matches that have quotation marks, but no in-text citation
- **0** Cited and Quoted 0%
  Matches with in-text citation present, but no quotation marks

Top Sources

7% Internet sources
5% Publications
6% Submitted works (Student Papers)

Top Sources

The sources with the highest number of matches within the submission. Overlapping sources will not be displayed.

1	Internet	pubmed.ncbi.nlm.nih.gov 2%
2	Student papers	Krea University on 2026-05-23 <1%
3	Internet	www.mdpi.com <1%
4	Student papers	IIT Delhi on 2019-05-28 <1%
5	Internet	www.researchsquare.com <1%
6	Internet	link.springer.com <1%
7	Internet	mdpi-res.com <1%
8	Publication	Prasanta Kumar Panda, Benudhar Sahoo, V. Sureshkumar, Ekaterina Dmitrievna ... <1%
9	Internet	anjaneyauniversity.ac.in <1%
10	Student papers	Sri Sathya Sai Institute of Higher Learning on 2017-04-06 <1%

11 Publication
Pichitchai Butnoi, Supalak Manotham, Pharatree Jaita, Chamnan Randorn, Gobw... <1%

12 Internet
pure.kfupm.edu.sa <1%

13 Student papers
National University of Singapore on 2019-11-06 <1%

14 Student papers
Indian Institute of Technology Guwahati on 2020-01-29 <1%

15 Internet
pdf.benchchem.com <1%

16 Internet
www.coursehero.com <1%

17 Student papers
Southern Taiwan University of Science and Technology on 2019-05-03 <1%

18 Publication
Xi Zou, Lu You, Weigang Chen, Hui Ding, Di Wu, Tom Wu, Lang Chen, Junling Wan... <1%

19 Internet
www.tdx.cat <1%

20 Publication
L Ceresara. Superconductor Science and Technology, 08/1996 <1%

21 Publication
Satheesh R, Meenu Venugopal, Anusree S. P, Dhanya V. S, H. Padma Kumar. "Opti... <1%

22 Student papers
The University of Manchester on 2024-09-03 <1%

23 Internet
www.hindawi.com <1%

24 Internet
www.scielo.br <1%

25 Publication

Vijaya Lakshmi Garlapati, Nitchal Kiran Jaladi, Nagamani Sangula. "Exploring the ... <1%

26 Internet

ethesis.nitrkl.ac.in <1%

27 Publication

Caixia Li, Tianqi Li, Chenglong Li, Nan Ji, Peng Lu, Shuang Ren. "First-principles cal... <1%

28 Student papers

Indian Institute of Technology on 2025-07-25 <1%

29 Publication

N. Izyumskaya, Y.-I. Alivov, S.-J. Cho, H. Morkoç, H. Lee, Y.-S. Kang. "Processing, Str... <1%

30 Student papers

University of Ulsan on 2015-10-02 <1%

31 Publication

Zhao, Yingying, Jiping Wang, Lixue Zhang, Xiujing Shi, Shujuan Liu, and Dawei Zh... <1%

32 Internet

cyberleninka.org <1%

33 Internet

honors.libraries.psu.edu <1%

34 Internet

mts.intechopen.com <1%

35 Internet

solid.fizica.unibuc.ro <1%

36 Internet

www.mri.psu.edu <1%

37 Internet

www.setaram.eu <1%

Study of Electrical Properties of Dy^{3+} doped $SrBi_2Nb_2O_9$ Aurivillius ceramic for electronic applications

A DESSERTATION REPORT

SUBMITTED IN PARTIAL FULFILLMENT OF THE REQUIREMENTS FOR THE AWARD OF THE DEGREE OF

MASTERS OF SCIENCE IN PHYSICS

Submitted by:

TARUNA
2024/MSCPHY/37

DIVYANSH RANJAN VARSHNEY
2024/MSCPHY/58

Under the supervision of
DR. RENUKA BOKOLIA
(Assistant Professor)

DEPARTMENT OF APPLIED PHYSICS

DELHI TECHNOLOGICAL UNIVERSITY

(Formerly Delhi College of Engineering)

Bawana Road, Delhi – 110042

MAY, 2026

DEPARTMENT OF APPLIED PHYSICS

DELHI TECHNOLOGICAL UNIVERSITY

(Formerly Delhi College of Engineering)

Bawana road, Delhi – 110042

CANDIDATE'S DECLARATION

We, **Taruna**, Roll No. **24/MSCPHY/37** and Divyansh Ranjan Varshney, Roll No. **24/MSCPHY/058** students of M.Sc. Physics here by declare that the project Dissertation titled "Study of Electrical Properties of Dy^{3+} doped $SrBi_2Nb_2O_9$ Aurivillius ceramic for electronic applications" which is submitted by us to the Department of Applied Physics, Delhi Technological University, Delhi in partial fulfilment of the requirement for the award of the degree of Master of Science, is original and not copied from any source without proper citation. This work has not previously formed the basis for the award of any Degree, Diploma Associateship, Fellowship or other similar title or recognition.

Place: Delhi	Taruna	Divyansh Ranjan Varshney
Date: 29/5/26	(24/MSCPHY/37)	(24/MSCPHY/058)

2 This is to certify that the student has incorporated all the corrections suggested by the examiners in the thesis and that the statement made by the candidate is correct to the best of our knowledge

Dr. Renuka Bokolia
(Assistant Professor)

DEPARTMENT OF APPLIED PHYSICS

DELHI TECHNOLOGICAL UNIVERSITY

(Formerly Delhi College of Engineering)

Bawana Road, Delhi-110042

CERTIFICATE

I, hereby certify that the Project Dissertation titled " **Study of Electrical Properties of Dy^{3+} doped $SrBi_2Nb_2O_9$ Aurivillius ceramic for electronic applications**" which is submitted by **Taruna**, Roll No. **24/MSCPHY/37** and **Divyansh**, Roll No. **24/MSCPHY/058**, Department of Applied Physics, Delhi Technological University, Delhi in partial fulfilment of the requirement for the award of the degree of Master of Science, is a record of the project work carried out by the students under my supervision. To the best of my knowledge this work has not been submitted in part or full for any Degree or Diploma to this University or elsewhere.

Place: Delhi **Dr. Renuka Bokolia**

Date: 29/05/2026

ACKNOWLEDGEMENT

I would like to express my indebtedness and deepest sense of regard to my supervisor, **Dr. Renuka Bokolia**, Assistant Professor, Department of Applied Physics, Delhi Technological University for providing her incessant expertise, inspiration, encouragement, suggestions, and this opportunity to work under her guidance. I am thankful for the constant help provided at every step of this project by **Surya Pratap Singh**, Department of Applied Physics, Delhi Technological University. I am also thankful to my family and colleagues for their invaluable support, care and patience during this project. Lastly, I would thank Delhi Technological University for providing such a wonderful opportunity of working on this project.

ABSTRACT

The effect of Dy^{3+} substitution on the structural, dielectric and ferroelectric properties of $SrBi_{(2-x)}Dy_xNb_2O_9$ (SBN) (x=0.00,0.02,0.04,0.06) was systematically investigated, and the samples were synthesized using the conventional solid-state reaction method. X-ray diffraction (XRD) confirmed the formation of a single-phase orthorhombic structure, indicating successful incorporation of Dy^{3+} into the lattice. The substitution of Dy^{3+} caused systematic variations in lattice parameters and unit cell volume, suggesting localized structural distortion. Scanning electron microscopy (SEM) revealed a plate-like grain morphology with random orientation, characteristic of layered perovskite systems. FTIR spectroscopy confirms bands are present at 816 cm^{-1}, 612 cm^{-1}, and 454 cm^{-1}. Dielectric studies show well-defined ferroelectric characteristics with low dielectric loss. The dielectric constant (ε) was observed to be 160 for undoped SBN ceramic. The Polarization-Electric field (P-E) hysteresis measurements confirmed the ferroelectric behavior of all compositions. The remanent polarization was recorded as highest at 4% (x=0.04), and 2Pr was 7.95 μC/$cm^{2,}$ whereas the coercive field 2Ec was 63.05 kV/cm. The variation in remanent polarization (Pr) and coercive field (Ec) with Dy^{3+} content indicates that dopant concentration significantly influences ferroelectric characteristics. Temperature-dependent PE loops indicate a stable ferroelectric response over a wide temperature range, 30°C to 180°C, with improved polarization. Good polarization retention with minute variations in remanent polarization (Pr) and coercive field (Ec) up to 10000 switching cycles, confirming good fatigue endurance and stability. Analysis of leakage current up to 10000 switching cycles reveals good insulating behaviour of the material with reduced defects and hence exhibits good electrical stability. Overall, Dy^{3+} substitution enhances structural stability, ferroelectric switching, and dielectric properties, making them useful in energy storage and sensing applications.

Keywords: $SrBi_2Nb_2O_9$ (SBN), Dy^{3+} doping, Solid-state reaction method, X-ray diffraction, Scanning electron microscopy, Ferroelectric properties, Dielectric properties.

Table of Contents

Page number

List of Figures

List of tables

Abbreviations

SBN	$SrBi_2Nb_2O_9$
SBND2	$SrBi_{1.98}Dy_{0.02}Nb_2O_9$
SBND4	$SrBi_{1.96}Dy_{0.04}Nb_2O_9$
SBND6	$SrBi_{1.94}Dy_{0.06}Nb_2O_9$
SBND8	$SrBi_{1.92}Dy_{0.08}Nb_2O_9$
SBND10	$SrBi_{1.90}Dy_{0.10}Nb_2O_9$

CHAPTER-1

INTRODUCTION

1.1 Background and Historical Context

The history of Aurivillius Ceramics starts in the year 1949, when Swedish chemist Bengt Aurivillius synthesized a unique oxide and published a paper on it [1]. Before 1990, research focused on compounds such as PZT, which have low remnant polarization and high Curie temperature, but these materials are harmful to the environment. A significant breakthrough was achieved when researchers at the Symmetrix company, based in Seattle, discovered compounds such as Strontium Bismuth Niobate $SrBi_2Nb_2O_9$(SBN) and Strontium Bismuth Tantalate $SrBi_2Ta_2O_9$ (SBT), which have high remnant polarization and less degradation over time than PZT. These materials exhibit fatigue-free behaviour under applied electric fields. This discovery paved the way for a non-volatile memory storage known as Fe-RAM.

Over the last two decades, environmental regulations have tightened, making the industrial use of compounds like PZT unsustainable, necessitating the shift to lead-free ceramics. The ability of Aurivillius ceramics to work under extreme conditions makes them suitable for applications in nuclear power plants and aerospace systems.

Today, research is focused on the spectroscopic characterization of these compounds, which helps to evaluate their structural integrity. Rare earth doping of elements has been investigated in host materials to enhance electrical and optical properties. Furthermore, A-site and B-site engineering have been explored to reduce leakage current and maximize remanent polarization to improve the quality of electrical components.

1.2 Aurivillius Ceramics

Aurivillius ceramics are an important class of ceramics that belong to Bismuth Layered Ferroelectric Structures (BLSF). They have excellent piezoelectric, ferroelectric, and dielectric properties. They have a high Curie temperature and high resistance to polarization fatigue under the applied electric field, making them ideal for high-temperature sensors and Ferroelectric

Random Access Memory (Fe-RAM). The general formula for Aurivillius ceramics is $(Bi_2O_2)^{2+}(A_{m-1}B_mO_{3m+1})^{2-}$.

1.3 Ferroelectric ceramics

Ferroelectric ceramics have self-generated electric polarization which can be reversed by applying an electric field, this phenomenon is known as ferroelectricity. The perovskite structure is represented as ABO_3, where A is the larger cation, for example, Ba^{2+} in $BaTiO_3$ and B is the smaller cation, for example, Nb^{5+} in KNN. Because of these traits, they are used in sensors, data storage, actuators and ultrasound devices

1.4 $SrBi_2Nb_2O_9$ (SBN) Ceramic

In this study, $SrBi_2Nb_2O_9$ (SBN) ceramic is selected as the host material and doped with Dy^{3+} [2]. Structural analysis of $SrBi_2Nb_2O_9$ (SBN) reveals a highly crystalline material consisting of two distinct structural blocks within the unit cell. The perovskite-like blocks comprise $(SrNb_2O_7)^{2-}$ layers, where strontium and niobium occupy the A- and B-sites of the NbO_6 octahedra, respectively. Interleaved $(Bi_2O_2)^{2+}$ sheets separate the perovskite blocks, acting as insulating layers between them [3].

SBN is a lead-free ceramic. Its eco-friendly nature makes it more suitable to use as compared to traditional materials like PZT. Due to the layered structure of SBN ceramic, the electrical and physical properties are highly directional, and there is a tiny shift that creates an electrical dipole without any external field being applied. This behaviour arises due to the spontaneous polarization inside the crystal lattice of SBN ceramic. Furthermore, doping this host material with rare earth elements or f-block elements like Er^{3+}, Dy^{3+}, and La^{3+} enhances its optical and electrical properties [4].

1.5 Rare earth doping strategy

Dy^{3+} was selected as a dopant due to its ionic radius of 0.912 Angstrom which is comparable to that of Bi^{3+} (1.03 Angstrom), facilitating the substitution of the bismuth without significant lattice distortion in the SBN ceramic. The present study aims to systematically investigate the effect of Dy3+ substitution on the structural, morphological, spectroscopic, ferroelectric, and dielectric properties of $SrBi_{(2-x)}Dy_xNb_2O_9$ ceramics.

19 Structural and electrical characterizations, including X-Ray Diffraction (XRD), Scanning Electron Microscopy (SEM), and Polarization-Electric field (PE) hysteresis loops, were performed. Frequency-dependent dielectric measurements were performed to investigate the dielectric behaviour and defect dynamics at room temperature. Moreover, Fourier Transform Infrared Spectroscopy (FTIR) was employed to identify bond characteristics and vibrational modes of the ceramic lattice.

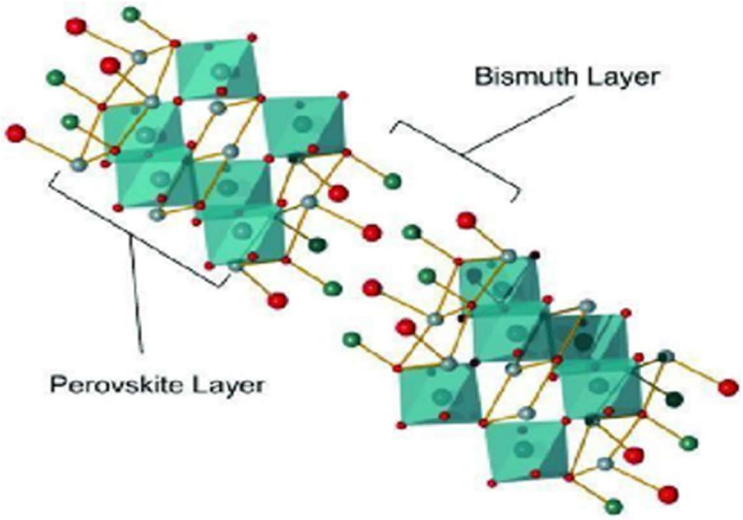

***Figure 1**: Bismuth Layered Structure Ferroelectric (BLSF) materials*

CHAPTER -2

SYNTHESIS PROCESS

2.1 Solid State Reaction Method (SSR)

SSR method is the standard and widely used technique for the preparation of ceramic powders. The method involves weighing of all the precursors in the stoichiometric ratio, to ensure uniformity and then the precursors are well mixed or grinned for long durations with ethanol to attain uniformity. After this the powders are calcined at high temperatures to form the fine powder and polyvinyl alcohol (PVA) was added in the calcined powder and then it was converted to round pellets with the help of the hydraulic press the powder is converted into round pallets. These pallets are then sintered at a very high temperature for specific duration of time. Now these sintered pallets are being used for various characterizations, like XRD, SEM, PE, Dielectric, etc., with the help of the characterization results, the of study various electrical properties of the respective material can be done.

2.2 Synthesis of SBN with Dy^{3+}

In the particular study, Dy^{3+} doped $SrBi_{(2-x)}Dy_xNb_2O_9$ (x=0.00,0.02,0.04,0.06), was prepared with process called the solid-state reaction (SSR) method. In this process, the precise weighing of the precursors of SBN, i.e., Bismuth Oxide (Bi_2O_3), Strontium Carbonate ($SrCO_3$), Dysprosium Oxide (Dy_2O_3), and Niobium (V) Oxide (Nb_2O_5) in the stoichiometric ratio for 15 g sample, respectively is done. Typically, the mixing is performed using a mortar and pestle for small quantities or a ball mill for larger amounts to ensure homogeneity. Here materials were then mixed with the help of an Agate mortar pestle with ethanol for 5 hours in order to get a uniform structure balance till they become a dry powder. Now this powder is calcined for 3 hours at a temperature of 950°C in a muffle furnace. 5wt% polyvinyl alcohol was added in the calcined powder and this powder is then converted to round pellets with a pelletizer at pressure around 50 kPa for 2 minutes. Then these

round-shaped pallets are sintered at a temperature of 1050°C for 3 hours. Now these sintered pallets are being used for various characterizations, like XRD, SEM, PE, Dielectric, etc., with the help of the characterization results, one can study various electrical properties of the respective material.

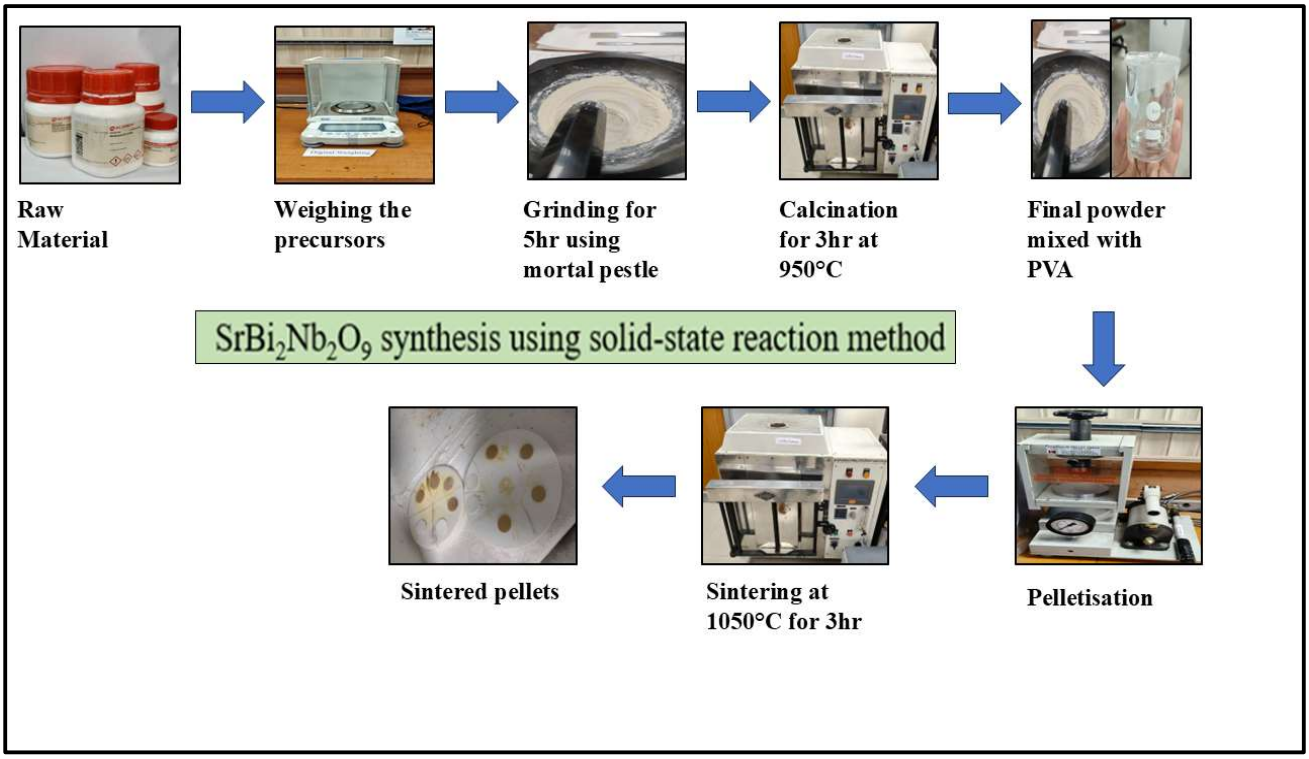

***Figure 2**: Schematic diagram for the synthesis of $SrBi_{(2-x)}Dy_xNb_2O_9$ ceramics using the solid-state reaction method for various dopant concentrations*

CHAPTER -3

CHARACTERIZATION RESULTS AND DISCUSSIONS

3.1 Basis of X-ray diffraction (XRD) techniques

The phase identification and crystal structure analysis of Dy^{3+} doped $SrBi_{(2-x)}Dy_xNb_2O_9$ (x=0.00,0.02,0.04,0.06) ceramics were carried out using X-ray diffraction (XRD) techniques, which are essential for determining the crystalline phases present in the samples and providing insights into their structural characteristics. The XRD patterns were obtained using a Bruker D8 Discover X-Ray Diffractometer, a sophisticated instrument capable of delivering high-resolution diffraction data. The samples were prepared by grinding the sintered pellets into fine powders, which were then placed on a sample holder for analysis. The XRD measurements were conducted over a range of angles (typically 2θ) to capture the diffraction peaks associated with various crystalline phases.

The resulting XRD patterns allowed for the identification of the crystalline phases present in both pure $SrBi_2Nb_2O_9$ and the Dy^{3+} doped variants. By comparing the observed diffraction peaks with standard reference patterns from databases such as the Joint Committee on Powder Diffraction Standards (JCPDS), researchers could confirm the presence of specific phases and assess any changes in crystallinity due to doping.

The analysis provided valuable information regarding the lattice parameters, crystallite size, and overall structural integrity of the materials, which are crucial for understanding their ferroelectric and optical properties.

3.2 XRD Results

X-Ray Diffraction (XRD) of the Dy^{3+}doped $SrBi_{(2-x)}Dy_xNb_2O_9$ (SBN)(x = 0.02,0.04,0.06) ceramic crystal structure is shown in Figure 2. Successful incorporation of the Dy^{3+} in the crystal structure of the host $SrBi_{(2-x)}Dy_xNb_2O_9$(SBN) is confirmed.

Dy^{3+} ions were substituted at the Bi^{3+} ions site in the crystal structure of $SrBi_{(2-x)}Dy_xNb_2O_9$ (x= 0.02,0.04,0.06). The doped and undoped ceramics were then analyzed through the XRD pattern. The graph between Bragg's angle (2θ), ranging from 10°- 80°, and intensity for all the compositions has been plotted and compared with the standard diffraction pattern of Strontium Bismuth Niobate $SrBi_2Nb_2O_9$ (SBN) that is the JCPDS data (#00-049-0607) as shown in Figure 2. X-ray diffraction confirms that the SBN formed is in a single phase with an A_{21} atom group, with no secondary peaks observed. Dy^{3+} ions doping in the crystal did not introduce defects as compared to the pure sample and successfully retained the orthorhombic structure. The most prominent peak shown in the XRD pattern is (115) for all the given compositions.

With increasing Dy^{3+} concentration, a slight shift is observed around 28° in left direction, attributed to the difference between the ionic radii of Dy^{3+} (0.912 Å) and Bi^{3+} ion (1.03 Å). This indicates lattice expansion of the crystal with unit cell volume increasing from 762.06 $Å^3$ to 765.14$Å^3$ at (x=0.04) as shown in **Table 1**. Upon increasing the doping to (x=0.06) Dy^{3+} ions, lattice distortion is observed, resulting in a reduction in volume of the unit cell (761.47 Å).

Regarding the distortion (b/a) as mentioned in **Table 1,** the crystal structure transitions from pseudo-tetragonal to orthorhombic structure. The density of the structures was calculated with Archimedes' principle as mentioned in **Table 1.** The structural parameters have been calculated using X-PowderX software as presented in **Table 1**. X-ray diffraction pattern results demonstrate enhancement in the properties. However, beyond optimal doping levels, distortion and degradation are observed [8,9,10,11].

Table1*: - Structural parameters of* $SrBi_{(2-x)}Dy_xNb_2O_9$ (SBN)

Samples ($SrBi_{(2-x)}Dy_xNb_2O_9$)				
Parameters	SBND0	SBND2	SBND4	SBND6
	x=0.00	x=0.02	x=0.04	x=0.06
a(Å)	5.5130	5.5272	5.5272	5.5112
b(Å)	5.5135	5.5189	5.5178	5.5101
c(Å)	25.074	25.0945	25.0970	25.0753
V($Å^3$)	762.06	765.48	765.14	761.47
Distortion (b/a)	1.0009	0.9985	1.0090	0.9998
Density (g/cm^3)	12.8075	5.2111	10.7913	3.9153

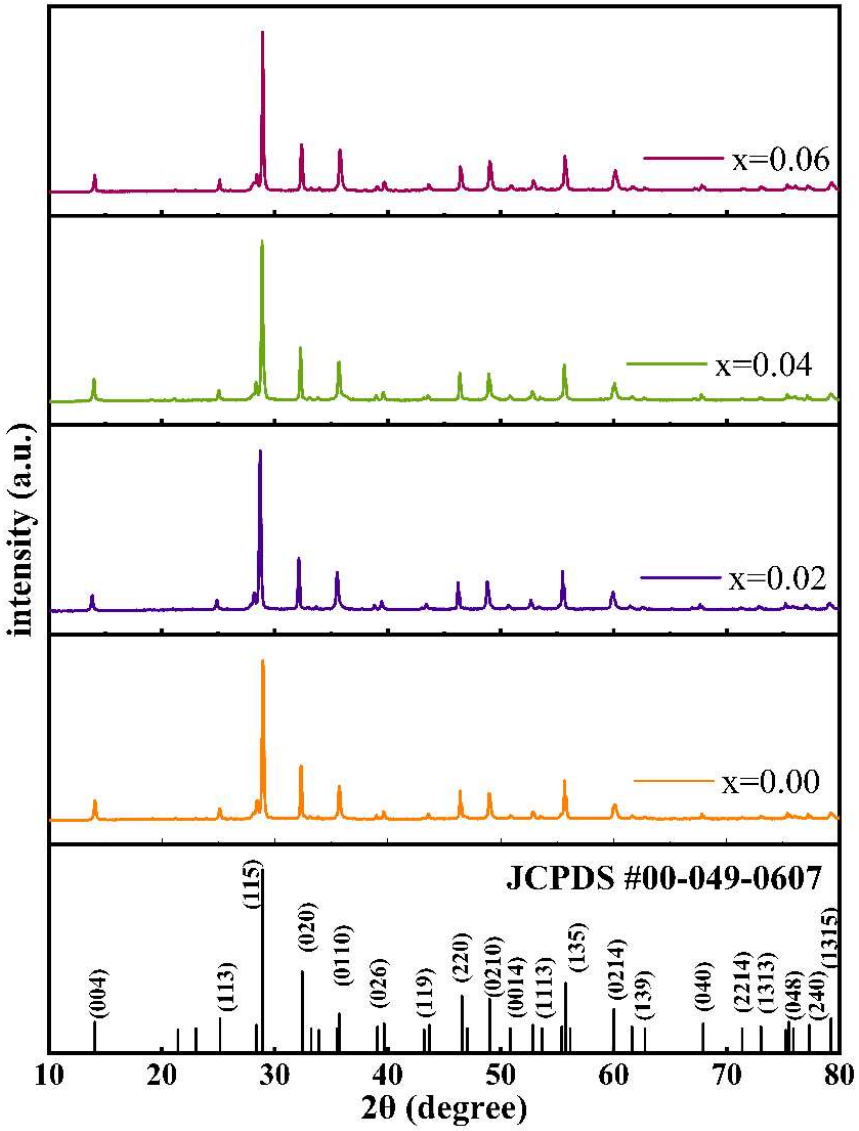

***Figure 3**: X-Ray Diffraction pattern of $SrBi_{(2-x)}Dy_xNb_2O_9$ (x=0.00,0.02,0.04,0.06)*

3.3 Structural Morphology Analysis (SEM)

Structural morphology analysis is an important part of materials research because it helps to understand how the material is built at the microscopic level and how the internal structure influences its overall behaviour. By using techniques such as scanning electron microscopy

(SEM), energy-dispersive X-ray spectroscopy (EDAX), and sometimes atomic force microscopy (AFM), one can observe the size, shape, and arrangement of grains or particles within a sample. These features play a major role in deciding how a ceramic conducts electricity, responds to stress, or interacts with external fields.

In a typical ceramic material, grains are tightly packed together, and the boundaries between them can affect electrical and mechanical performance. Morphological analysis allows us to see whether the grains are uniform, well-developed, or porous. For example, larger grains often indicate better crystallization, while smaller or irregular grains may suggest incomplete reactions or the presence of defects. The presence of pores or cracks can also influence conductivity and dielectric properties by interrupting the continuity of the structure.

Doping changes grain growth behaviour, alter density, or introduce local strain, all of which can be visually confirmed through SEM images. By comparing undoped and doped samples, one can easily identify whether the modification improved the microstructure or introduced unwanted irregularities.

3.4 Results of SEM

The analysis of Scanning Electron Microscope (SEM) images reveals the surface morphology of sintered pellets of $SrBi_{(2-x)}Dy_xNb_2O_9$ (SBN) (x=0.00). The SEM images are depicted below in Figure 3. $SrBi_{(2-x)}Dy_xNb_2O_9$ (SBN) ceramic exhibits a plate-like structure with random orientation, characteristic of BLSF material. Grain size was calculated using Image J software and corresponding histograms were plotted for each concentration of Dy^{3+}, i.e., (x=0.00,0.02, 0.04,0.06) [12].

The grain size of each concentration is 1.440 µm for no doping (x=0.00) of Dy^{3+}ion**,** 1.505 µm for (x=0.02) concentration of Dy^{3+} ion, 1.547µm for (x=0.04) of Dy^{3+} ion, and 1.323µm for (x=0.06) of Dy^{3+}ion. The average grain size is 1.4535µm. The highest value of grain size is at x=0.04 doping, indicating fewer defects in the crystal compared to other crystals due to its high grain size. Upon further increasing the concentration, distortion is observed due to the excessive doping, hence effective non-radiative energy transfer, resulting in a grain size of 1.323 µm. Therefore, x=0.04 doping or concentration of Dy^{3+} ion is identified as optimum for crystal growth and various electrical and optical properties of SBN ceramic.

SEM images confirm that the layered structures of SBN ceramic dominate the morphology of the crystal. At x=0.04, doping of the Dy^{3+} ion exhibits the highest structural enhancement of SBN ceramics [13,14,15].

Table 2: - *Grain size (μm) for SBN ceramic.*

Concentration	x=0.00	x=0.02	x=0.04	x=0.06
Grain size(μm)	1.440	1.505	1.547	1.323

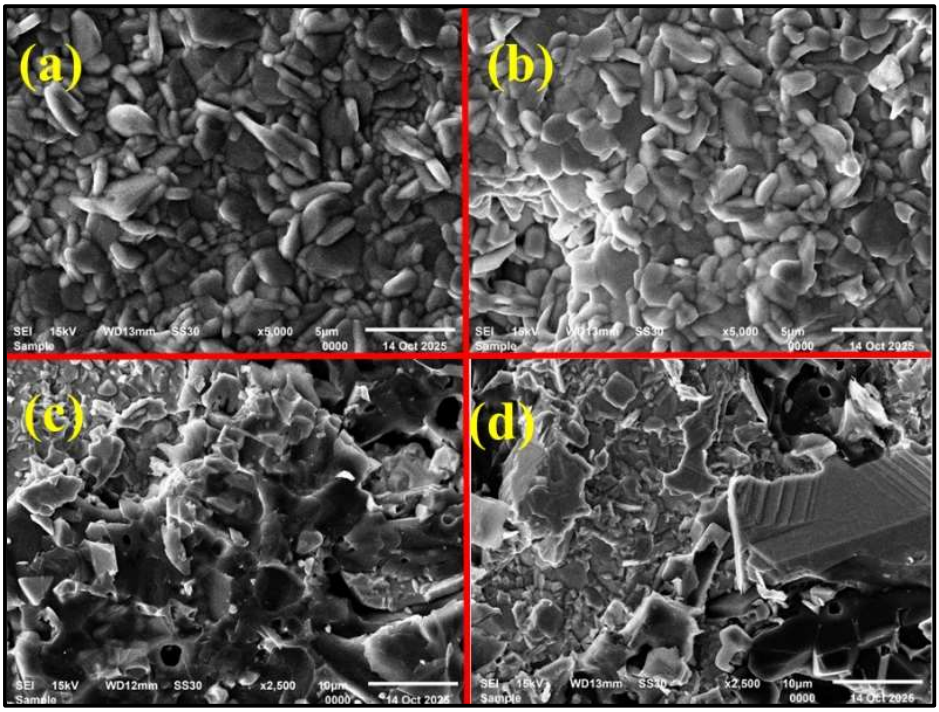

Figure 4(a-d): *SEM images of $SrBi_{(2-x)}Dy_xNb_2O_9$ (SBN) where x=0,0.02,0.04,0.06 respectively.*

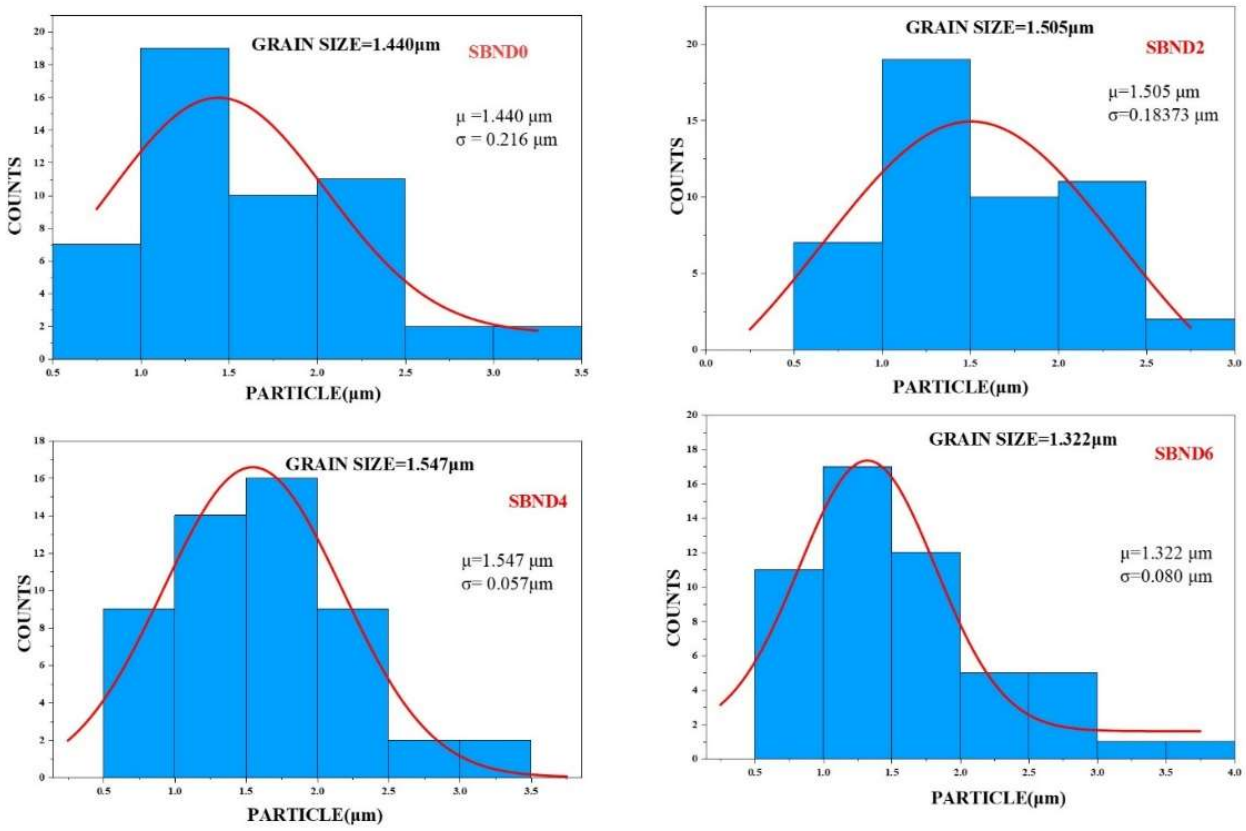

Figure 5(a-d). *Histograms used for calculations of grain size from the SEM images for each Dy^{3+} doped of $SrBi_{(2-x)}Dy_xNb_2O_9$ (SBN)ceramics: (a) undoped (x = 0.00), (b) x = 0.02, (c) x = 0.04, and (d) x = 0.06,*

3.5 FTIR (Fourier Transform Infra-Red spectroscopy)

FTIR spectroscopy involves recording the infrared spectrum of absorption of different types of solid, liquid, and gas materials. Various types of chemical bonds inside the structure absorb different types of frequencies. The resulting spectra are plotted on the transmission (%) versus wavenumber (cm^{-1}).

In our study of Dy^{3+} doped $SrBi_{(2-x)}Dy_xNb_2O_9$ (SBN) (x=0.00, 0.02,0.04,0.06), the following observations were recorded. The Fourier Transform InfraRed Spectrum Peak at 816 cm^{-1} represents a high frequency stretch of NbO_6 bonds, indicating that the bond present here has a shorter bond length, stronger and more rigid bonds are present in this region. Doping of Dy^{3+} ion in the Bravais lattice of $SrBi_{(2-x)}Dy_xNb_2O_9$ (SBN) ceramic confirms changes in the absorption in the FTIR spectra, with a sudden decrease in transmittance for x=0.02 concentration. Subsequently,

transmittance returns closer to its original position and a left shift is observed in the wavenumber(cm^{-1}) scale on the observed spectra of the doped ceramic of SBN [16].

The peak at 612 cm^{-1} represents the lower frequency region of NbO_6, which indicates it has a longer bond length compared to the bonds present in the region of the 816 cm^{-1}. Consequently, a longer bond length is present in the region and the bond strength of the bonds available in the region is relatively lower. Regarding the effect of Dy^{3+}, transmittance follows a similar trend as observed in the 816 cm^{-1}region, with an increase observed at x=0.04. Upon increasing to x=0.06, left shift in the peak is observed [17]. The peak at 454 cm^{-1} indicates overlapping of $(Bi_2O_2)^{2+}$ structures and oxygen atoms flexing or moving relative to the central niobium atom in the Bravais lattice. Furthermore, $(Bi_2O_2)^{2+}$ is sandwiched between the perovskite layers of the $(SrNb_2O_7)^{2-}$[18]. The absence of peaks between 2000-1000 cm^{-1} confirms a high-quality ceramic or crystal has formed.

These observations confirm that NbO_6 has a distorted octahedral structure in the Bravais lattice of SBN ceramic.

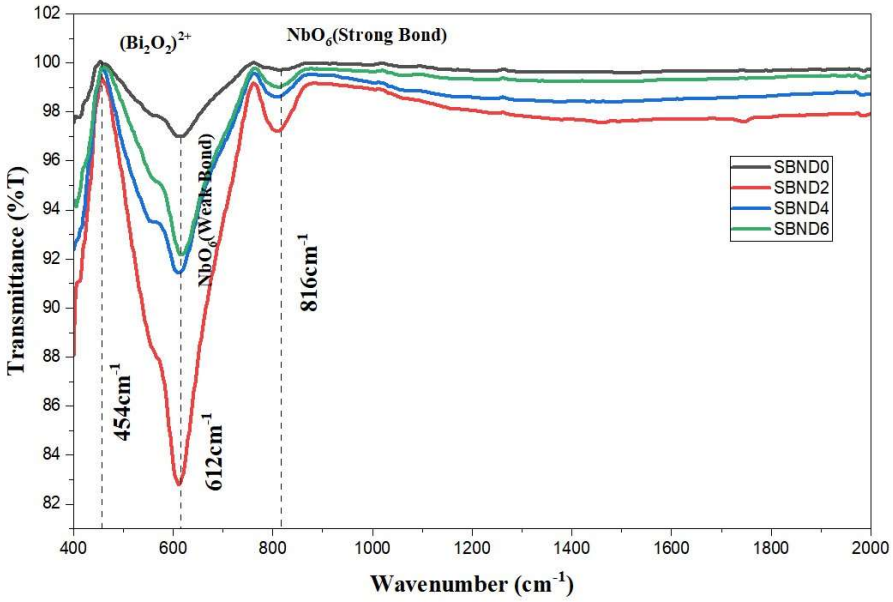

Figure 6: FTIR Spectra for the $SrBi_{(2-x)}Dy_xNb_2O_9$ (SBN) ceramic, where x=0.00 (undoped), x=0.02, x=0.04, x=0.06

3.6 Polarization-Electric field (PE) hysteresis loop

The Polarization–Electric field (P–E) hysteresis loop is one of the most important techniques to understand the ferroelectric behaviour of a material. It demonstrates how the electric polarization of a sample responds to an externally applied electric field.

In ferroelectrics, their polarization does not immediately return to zero once the field is switched off. Hence, creates a characteristic loop shape when polarization is plotted against the electric field, known as the hysteresis loop. From this loop, several key properties of the material can be extracted, like the remnant polarization (P_r) and coercive field E_c.

The remnant polarization (P_r) tells how much the polarization remains after removing the electric field, signifying the strength and stability of the ferroelectric domains.

The coercive field E_c represents the field required to switch the polarization direction, revealing how easily the domains can be reoriented. A wider loop usually suggests stronger ferroelectric behaviour, while a slimmer loop may depict weak polarization.

3.7 PE Loop Results

Polarization-electric field (PE) hysteresis loop is a fundamental characteristic property of ferroelectric materials, which provides information about the remanent polarization (P_r) and coercive field (E_c).

The remanent polarization (P_r) is the polarization left in the ferroelectric materials after the removal of the external electric field, whereas the coercive field (E_c) measures the electric field required to reduce the polarization of a material. PE loops for the composition $SrBi_{(2-x)}Dy_xNb_2O_9$ (SBN), where x=0, 0.02, 0.04, 0.06 are presented in Figure 6. Well-developed hysteresis loops confirm the ferroelectric nature of all compositions formed [19]. With increasing Dy^{3+} content, the remanent polarization (2Pr) increases up to an optimum level (x=0.04), as presented in **Table 3** leading to improved ferroelectric properties in the material. The undoped sample, SBND0 (x=0.00), exhibits a narrow and unsaturated loop with low remanent polarization ($2P_r$=2.94μC/cm^2). At x=0.02 (SBND2), the loop is open but not fully saturated compared to SBND0, with a slight increase in 2Pr value is observed($2P_r$=5.57μC/cm^2). At x=0.04 (SBND4) results in a well-developed and saturated loop with a high $2P_r$ value (7.95μC/cm^2). This indicates that x=0.04 doping sample SBND4 has a strong ferroelectric response, and with the best balance

of strong polarization, this makes it suitable for designing ferroelectric devices like capacitors and sensors. At higher Dy^{3+} concentration (x=0.06), the loop of SBND6 becomes narrow and contracts near the origin. Defects are generated due to which the dipoles are misaligned, resulting in a reduction of the value of remanent polarization to $2P_r = 1.53\mu C/cm^2$, significantly lower compared to other compositions and further results in degradation of ferroelectric properties of the material.

The coercive field (E_c) indicates domain stability; the higher the value of E_c indicates more stable domains and harder domain switching, whereas a lower E_c indicates unstable domains, referring to domain motion and easier switching. With increasing content of Dy3+, coercive field (2Ec) also increases as presented in Table 3 up to an optimum level (x=0.04). SBND0 exhibits a low 2Ec (36.82KV/cm), indicating easy switching of the domains with weak polarization, reflecting poor domain stability. At SBND2 (x=0.02), 2Ec=58.12KV/cm, reflecting improved domain stability and enhanced ferroelectric configuration. Further, at SBND4 (x=0.04), 2Ec=63.05KV/cm, indicating a balance between domain stability and switching, and thus is used for various applications. At x=0.06, (SBND6) 2Ec = 30.48 KV/cm, domain switching becomes easier, contributing to internal defects, resulting in degradation of ferroelectric behaviour.

The variation in Dy^{3+} concentration considerably affects the ferroelectric behavior of the $SrBi_{(2-x)}Dy_xNb_2O_9$ (SBN) ceramic. Therefore, SBND4 achieves the most refined ferroelectric properties with a value of remanent polarization $2Pr = 7.95\mu C/cm^2$ and $2E_c = 63.05KV/cm$. Hence, SBND4 can be used for various applications, such as capacitors, sensors, where both high polarization and easy switching are important [20,21,22].

The value of coercive field ($2E_c$) for all the compositions is presented in the table and the graph for PE loops for the composition $SrBi_{(2-x)}Dy_xNb_2O_9$ (SBN) where x=0, 0.02, 0.04, 0.06, has been plotted.

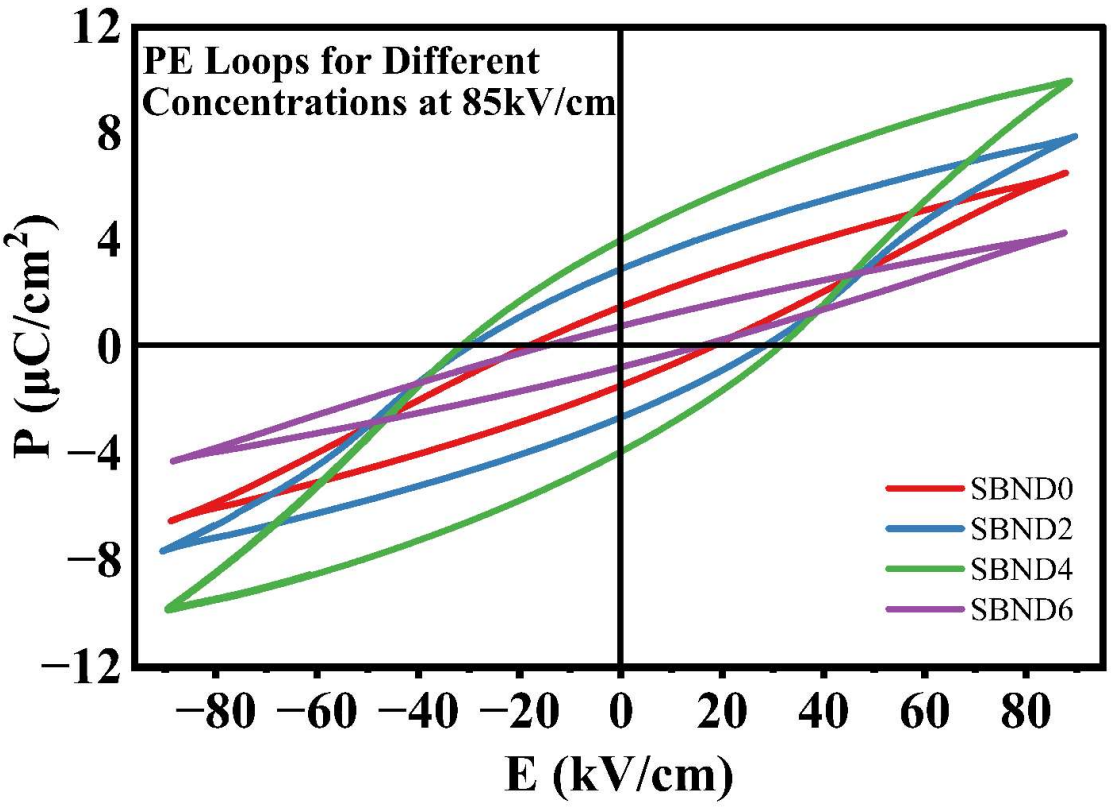

***Figure** 7: PE loops for the composition $SrBi_{(2-x)}Dy_xNb_2O_9$ (SBN) where x=0,0.02,0.04,0.06.*

***Table 3**: Calculated values of remanent polarization ($2P_r$) and coercive field ($2E_c$)*

Sno.	Polarization	SBND0	SBND2	SBND4	SBND6
1	2Pr (μC/cm^2)	2.94	5.57	7.95	1.53
2	2Ec (kv/cm)	36.82	58.12	63.05	30.48

3.7.1 Temperature-dependent PE Analysis

Temperature-dependent PE analysis reveals the material's macroscopic ferroelectric properties and thermal stability.

Temperature-dependent PE hysteresis loops were recorded for Dy^{3+} doped $SrBi_{(2-x)}Dy_xNb_2O_9$ compositions (x = 0.00,0.02,0.04,0.06) over a temperature range of 30°C to 180°C. The remnant polarization (Pr), maximum polarization (P_m), Coercive field (E_c) and maximum applied field (E_{max}) were extracted from the dataset of PE hysteresis loop.

At x=0.00(SBND0), the remnant polarization(P_r) is recorded as 0.368 μC/cm^2, and the maximum polarization (P_m) is 3.309 μC/cm^2 at 30°C. Both parameters increase steadily with rising temperature, attaining values of 4.386 μC/cm² and 7.790 μC/cm², respectively, at 180°C.

At x=0.02(SBND2), the values of P_r and P_m exhibit a notable increase owing to enhanced dipole alignment induced by Dy^{3+} ions in the SBN ceramics. At 30°C P_r and P_m are recorded as 2.723 μC/cm^2 and 7.310 μC/cm^2, respectively. At 180°C, P_r and P_m further increase to 9.709μC/cm^2,14.969 μC/cm^2, respectively. At x=0.04(SBND4), the values of P_r and P_m further increase; there is better alignment of dipoles as compared to SBND2. The values of P_r and P_m at 30°C are 4.091 μC/cm^2 and 8.091 μC/cm^2, respectively, while at 180°C they reach 11.542 μC/cm^2 and 15.095 μC/cm^2. For x=0.06, the values decrease compared to SBND4, which is attributed to excessive lattice distortion induced by over-substitution of Dy^{3+} at the Bi-site. The values at 30°C are 1.312 μC/cm^2 and 4.561μC/cm^2. At 180 °C, the respective values of P_r and P_m are 7.277μC/cm^2 and 11.213 μC/cm^2. These results establish that SBND4 (x = 0.04) exhibits the most favourable ferroelectric properties and thermal stability among all investigated compositions, identifying it as the most promising candidate for non-volatile ferroelectric memory device applications.

Talking about the temperature-dependent coercive field (E_c) it tell us about the thermal agitation of the dipole inside the ceramic material. In general, it decreases with an increase in temperature.

In our study of Dy^{3+} doped $SrBi_{(2-x)}Dy_xNb_2O_9$ compositions (x = 0.00,0.02,0.04,0.06))is recorded.

For x = 0.00 (SBND0), the coercive field (Ec) is 8.272 kV/cm at 30°C. It increases steadily with rising temperature, attaining a value of 40.373 kV/cm at 180°C.

For x = 0.02 (SBND2), the value of Ec exhibits a notable increase owing to enhanced dipole alignment induced by Dy^{3+} ions in the SBN ceramics. At 30°C, E_c is recorded as 30.931 kV/cm. At 180°C, Ec further increases to 40.206 kV/cm.

For x = 0.04 (SBND4), Ec decreases compared to SBND2, which is attributed to superior dipole ordering induced by Dy^{3+} substitution at the Bi-site. At 30°C, E_c is recorded as 18.161 kV/cm, while at 180°C it reaches 21.106 kV/cm.

For x = 0.06 (SBND6), Ec decreases compared to SBND4, which is attributed to excessive lattice distortion induced by over-substitution of Dy^{3+} at the Bi-site. At 30°C, E_c is recorded as 11.92 kV/cm. At 180°C, Ec attains a value of 21.741 kV/cm[23,24].

Based on these results, the SBND4 ceramic is the most suitable composition for non-volatile ferroelectric memory storage device. Data of the temperature run for the different compositions is given below in **Table 4.**

Table 4 :- *Remanent Polarizations and coercive field values for different composition of* $SrBi_{(2-x)}Dy_xNb_2O_9$ *(SBN) where x=0,0.02,0.04,0.06 at different temperatures*

Temperature(° C)	SBND0		SBND2		SBND4		SBND6	
	P_r (μC/cm^2)	E_c (kV/cm)	P_r (μC/cm^2)	E_c (kV/cm)	P_r (μC/cm^2)	E_c (kV/cm)	P_r (μC/cm^2)	E_c (kV/cm)
30	0.368	8.272	2.723	30.931	4.091	18.161	1.312	11.929
40	0.378	4.097	2.846	16.126	4.151	36.955	1.346	25.351
50	0.384	4.098	2.949	32.557	4.282	18.588	1.367	25.538
60	0.392	4.215	3.12	16.863	4.5	37.941	1.412	25.838
70	0.399	8.848	3.341	17.291	4.563	18.951	1.471	12.814
80	0.42	9.181	3.649	35.327	4.657	37.844	1.56	26.933
90	0.455	9.686	4.114	18.546	4.855	38.855	1.694	13.745
100	0.526	10.872	4.762	19.342	5.396	39.653	1.908	14.642
110	0.637	12.609	5.585	40.149	5.812	40.198	2.234	32.292
120	0.811	7.457	6.525	41.373	6.646	41.448	2.786	17.809
130	1.129	19.761	7.471	20.887	7.476	42.449	3.53	19.519
140	1.600	12.479	8.277	42.064	8.419	21.521	4.432	20.868
150	2.193	30.878	8.92	41.661	9.359	43.93	5.352	43.816
160	2.934	35.651	9.368	20.352	10.977	43.7	6.175	22.032
170	3.669	38.612	9.709	40.206	11.371	21.395	6.784	21.99
180	4.386	40.373	---------	--------	11.542	21.106	7.277	21.741

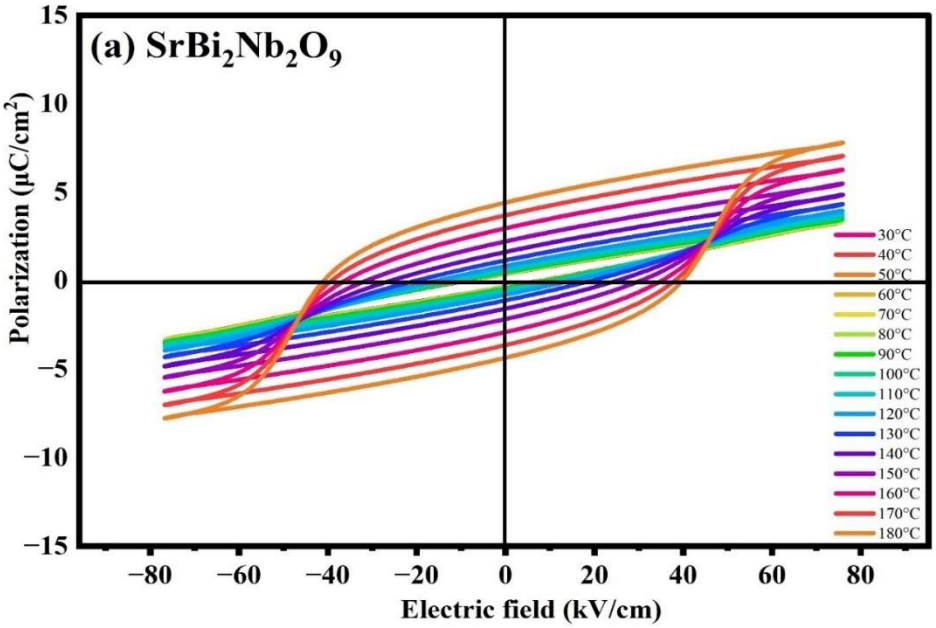
(a) SrBi2Nb2O9
Polarization (μC/cm2)
Electric field (kV/cm)
30°C
40°C
50°C
60°C
70°C
80°C
90°C
100°C
110°C
120°C
130°C
140°C
150°C
160°C
170°C
180°C

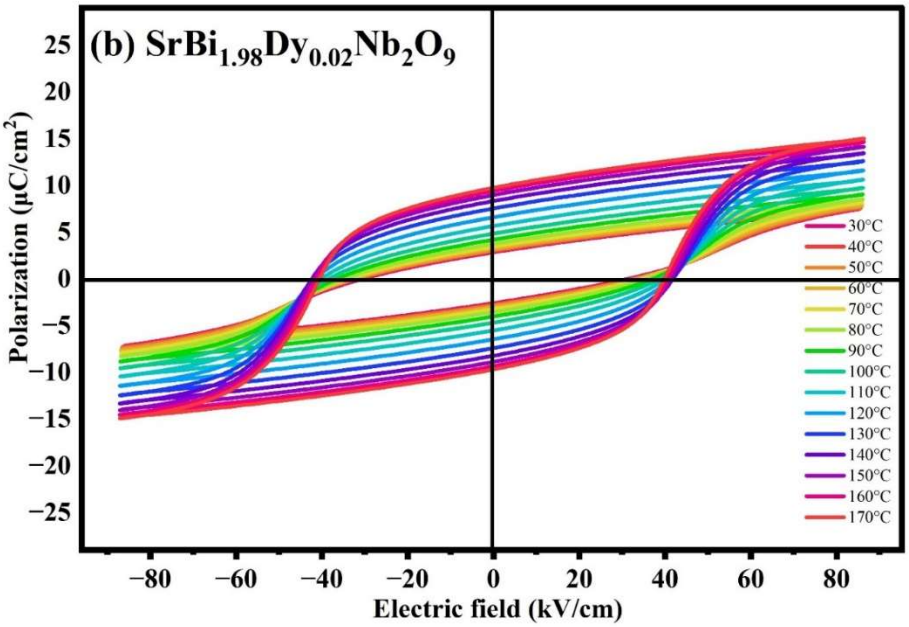
(b) SrBi1.98Dy0.02Nb2O9
Polarization (μC/cm2)
Electric field (kV/cm)
30°C
40°C
50°C
60°C
70°C
80°C
90°C
100°C
110°C
120°C
130°C
140°C
150°C
160°C
170°C

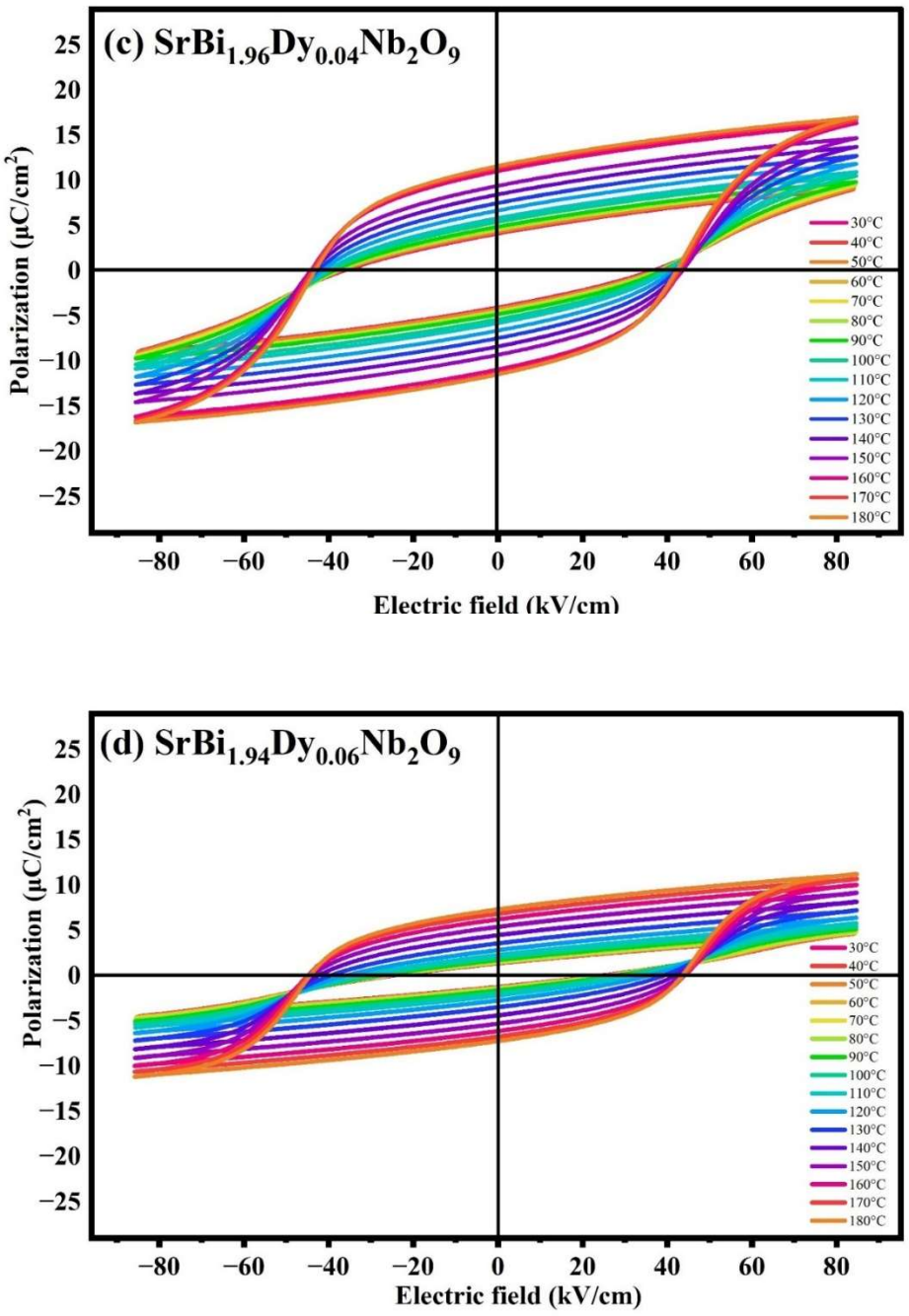

Figure 8(a-d): *Plots of temperature-dependent PE loop for each Dy^{3+} doped $SrBi_{(2-x)}Dy_xNb_2O_9$ (SBN) ceramics: (a) undoped (x = 0.00), (b) x = 0.02, (c) x = 0.04, and (d) x = 0.06.*

3.7.2 Fatigue analysis of PE loop

Fatigue test is a mechanism to be carried out to test the ferroelectric material to check how well it retains its remanent polarization after a million cycles of applied electric field. The gradual loss in remanent polarization is known as ferroelectric fatigue The gradual loss in remanent polarization is known as ferroelectric fatigue. When a ferroelectric ceramic is subjected to a large number of alternating electric field cycles, the domain walls responsible for polarization switching become increasingly pinned by accumulated space charges, oxygen vacancies, and structural defects at grain boundaries and electrode interfaces. As a result, the fraction of switchable polarization volume decreases gradually with increasing cycle number, leading to a measurable reduction in P_r. This phenomenon directly limits the operational lifetime of ferroelectric-based devices such as non-volatile ferroelectric random access memory (FeRAM), actuators, and sensors. Therefore, fatigue characterization is essential to check the practical application of the ceramic before it can be used in Fe-RAM devices to avoid the breakdown before using it.

In our study of Dy^{3+} doped $SrBi_{(2-x)}Dy_xNb_2O_9$ compositions (x = 0.00,0.02,0.04,0.06), a fatigue test was performed by applying a bipolar electric field over 10,000 cycles. The values of remanent polarization, coercive field and leakage current were recorded.

For SBND0(x=0.00), the values of remnant polarization are relatively stable regarding all cycles in which it was performed. The range of value of P_r is 0.37 μC/cm^2 to 0.377μC/cm^2. This confirms the fatigue-resistant nature of SBN ceramic. The coercive field also shows minimal variation during the scan and its range is 3.912 kV/cm to 4.059 kV/cm. Upon SBND2(x=0.02) the value of remnant polarization shows slight variation with increasing cycles. The minor defects are shown due to the incorporation of Dy^{3+} in the SBN ceramic. The range values of remnant polarization and coercive field are 2.35-2.682μC/cm^2, 27.514-30.288 kV/cm. For SBND4(x=0.04), the remnant polarization exhibits highly stable composition for all compositions throughout the entire cycling process. It confirms Dy^{3+} establishes the perfect domain wall structure, resulting in superior fatigue resistance. The coercive field also remains constant throughout the entire process. Upon increasing the concentration at x=0.06(SBND6), a gradual decrease is observed during the cycles of the applied electric field. It happens due to the lattice distortion caused by the excessive

doping of Dy^{3+}. This confirms that the excessive doping of Dy at the Bi-site in the SBN ceramic also deteriorates the fatigue resistance of the ceramic.

Based on these results, SBND4 exhibits the most stable fatigue resistance behaviour among all other compositions, which makes it ideal for a non-volatile Fe-RAM memory storage device[25,26,27,28].

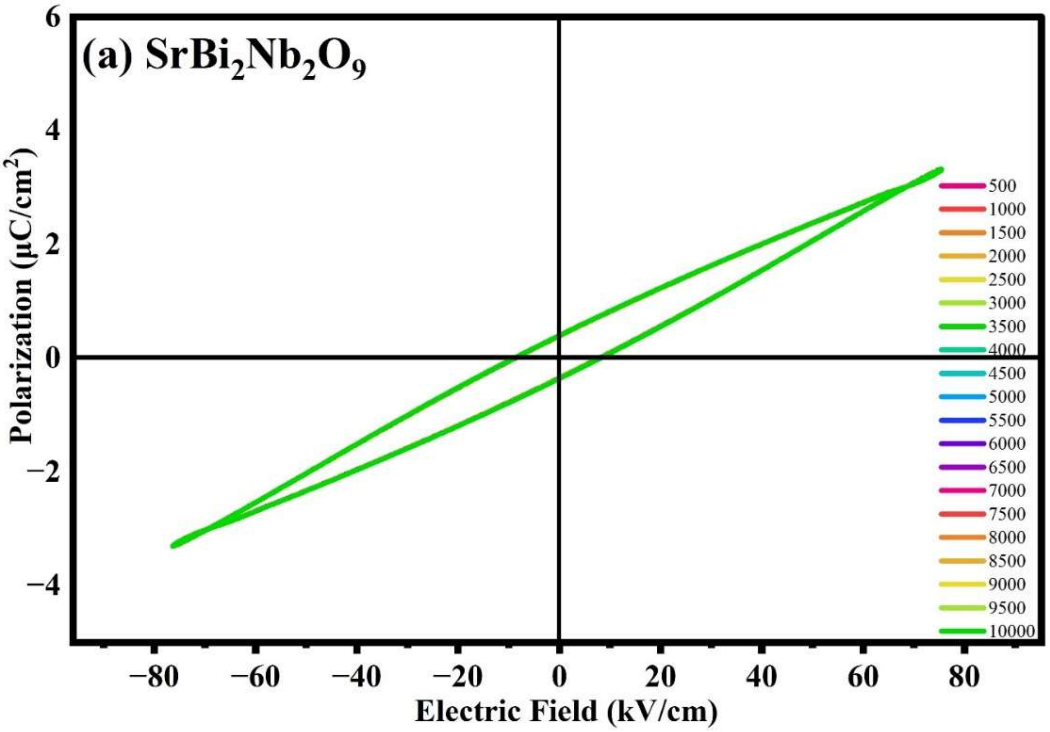

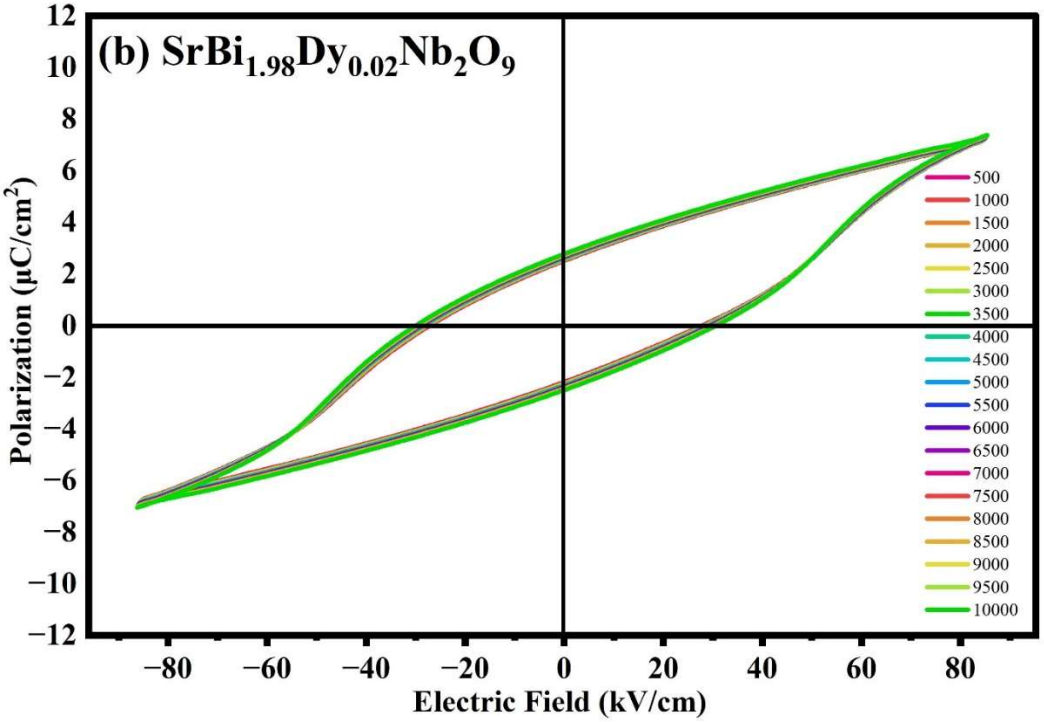
(b) SrBi1.98Dy0.02Nb2O9
Polarization (μC/cm2)
Electric Field (kV/cm)
500
1000
1500
2000
2500
3000
3500
4000
4500
5000
5500
6000
6500
7000
7500
8000
8500
9000
9500
10000

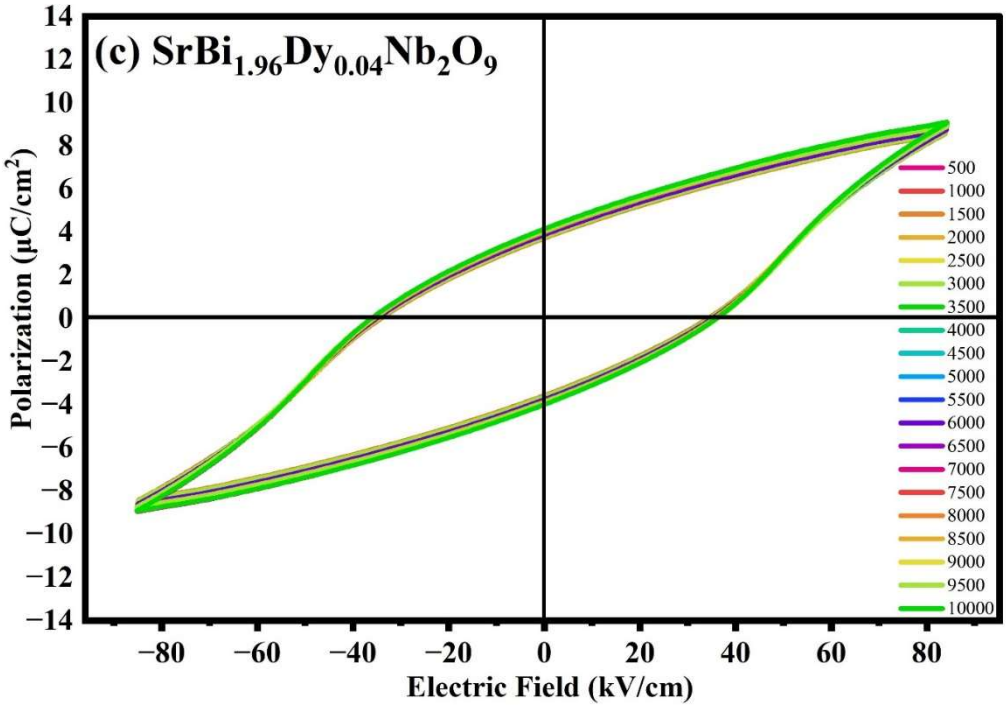
(c) SrBi1.96Dy0.04Nb2O9
Polarization (μC/cm2)
Electric Field (kV/cm)
500
1000
1500
2000
2500
3000
3500
4000
4500
5000
5500
6000
6500
7000
7500
8000
8500
9000
9500
10000

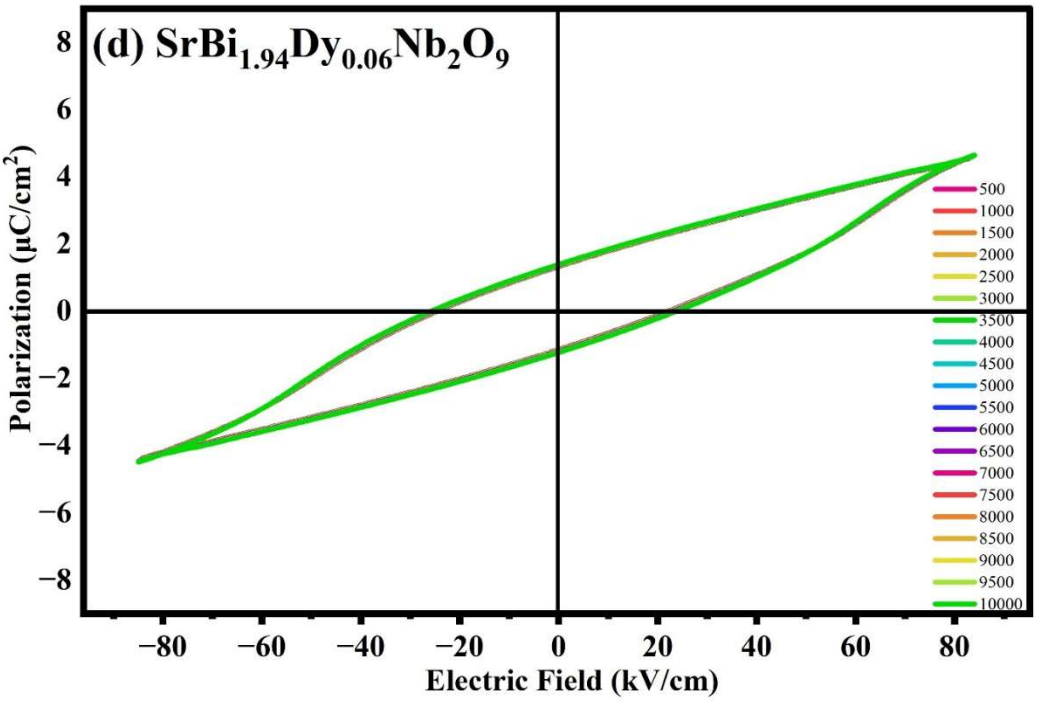

***Figure 9(a-d)**: plots of fatigue analysis of PE loop for each Dy^{3+} doped $SrBi_{(2-x)}Dy_xNb_2O_9$ (SBN)ceramics: (a) undoped (x = 0.00), (b) x = 0.02, (c) x = 0.04 and (d) x = 0.06.*

3.7.3 Leakage current

The unwanted flow of electric current inside a ferroelectric material under an applied electric field is due to the movement of charge carriers, such as oxygen vacancies, electrons, and holes, through the ceramic lattice is known as leakage current. If the leakage current is high, then it leads to a distorted PE loop for the ferroelectric materials. It indicates that poor insulating behaviour results in detorting the polarization switching of the ferroelectric materials. Therefore, low and stable leakage current is required for reliable ferroelectric device applications, like non-volatile Fe-RAM and other memory devices.

In the present study of Dy^{3+} doped $SrBi_{(2-x)}Dy_xNb_2O_9$ compositions (x = 0.00,0.02,0.04,0.06), the following observations were made in the domain of leakage current. At x=0.00 (SBND0) the value of leakage current is highly stable and lies between 0.100 mA to 0.102 mA over 10,000 cycles of applied electric field. The increase observed in leakage current is due to the accumulation of charges on the interface of electrodes and grain boundaries. For x=0.02 (SBND2), the range of

leakage current lies between 0.138 mA to 0.140 mA for the applied electric field over the electric field for 10,000 cycles. An increment in leakage happens due to the substitution of Dy^{3+} at the Bi-site in the lattice of $SrBi_{(2-x)}Dy_xNb_2O_9$ ceramic. Nevertheless, the variation in leakage current value is in an acceptable range, confirming the poor insulating behaviour for the compositions. Upon increasing the concentration to x=0.04(SBND4), the leakage current is thoroughly uniform at 0.138 mA, which shows the ferroelectric behaviour of the sample does not deteriorate on applying bipolar cycles of electric field over 10,000 cycles. It confirms the good insulating behaviour of SBND4. This stable leakage current behaviour further supports the superior fatigue resistance of the SBND4 composition, consistent with the stable P_r observed throughout the cycling process. Further increment to x=0.06(SBND6) of Dy^{3+} at the Bi-site in the lattice of $SrBi_{(2-x)}Dy_xNb_2O_9$ ceramic, the variation in the leakage current in the range of 0.104 mA to 0.105 mA over 10,000 bipolar switching cycles. This trend is observed due to the excessive doping of Dy^{3+}, which results in lattice distortion and distortion of the PE loop because of overaccumulation of the charge carriers[29,30,31].

Based on these results, SBND4 is the most suitable candidate for memory devices like Fe- RAM.

The combined plots for remnant polarization (P_r), Coercive Field (E_c), Maximum polarization (P_m) and leakage current (mA) are shown below in Figure 10

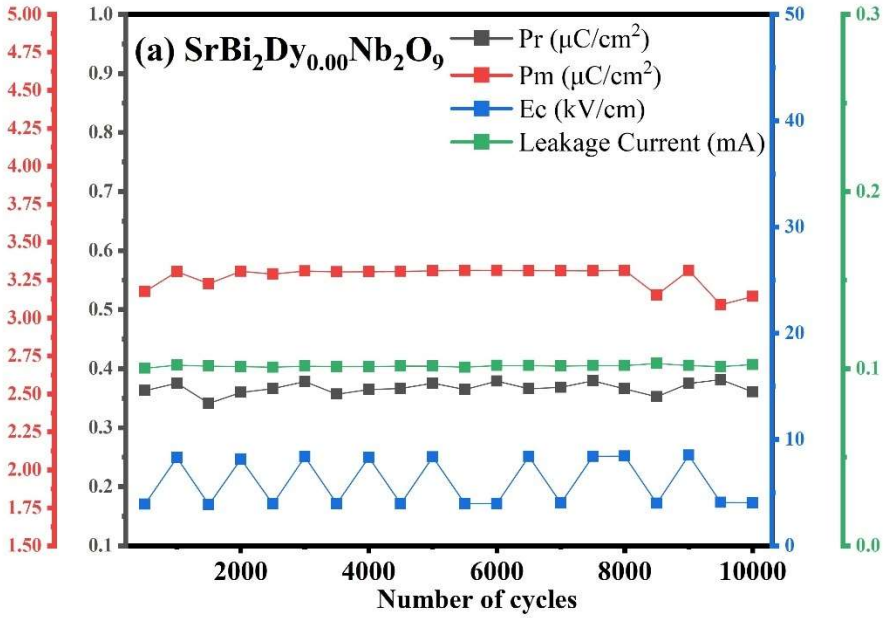

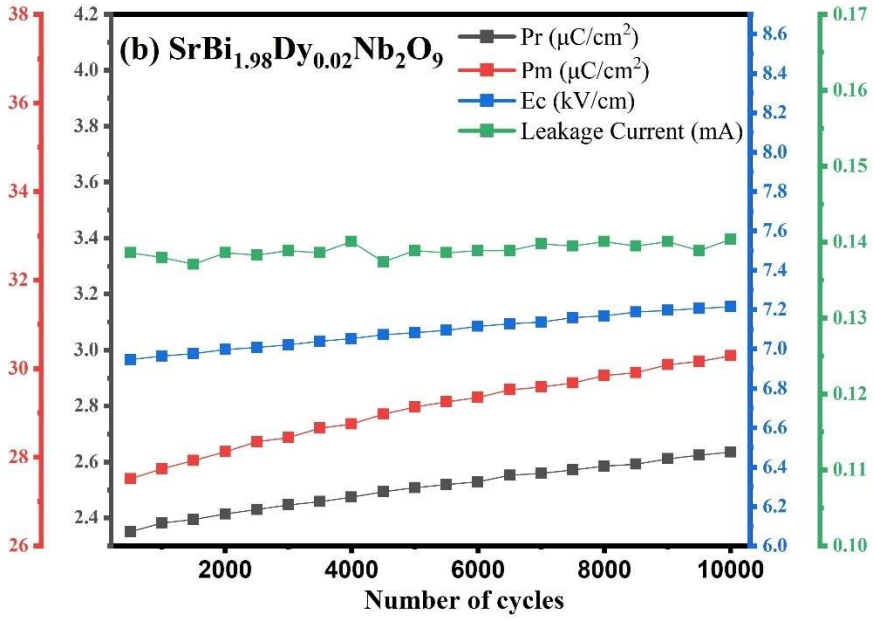
(b) SrBi1.98Dy0.02Nb2O9
Pr (μC/cm2)
Pm (μC/cm2)
Ec (kV/cm)
Leakage Current (mA)
Number of cycles

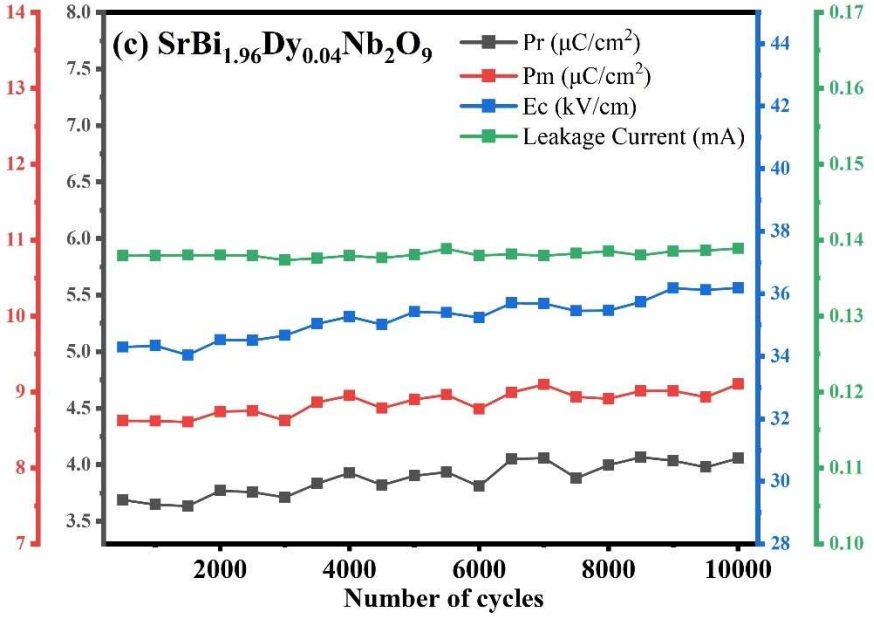
(c) SrBi1.96Dy0.04Nb2O9
Pr (μC/cm2)
Pm (μC/cm2)
Ec (kV/cm)
Leakage Current (mA)
Number of cycles

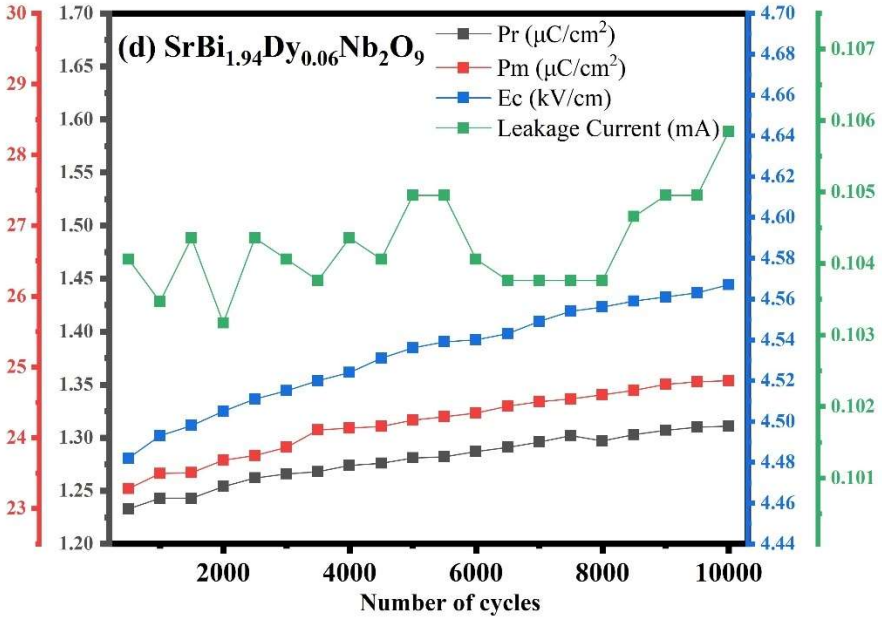

***Figure 10(a-d)**: The combined plots for remnant polarization (P_r), Coercive Field (E_c), Maximum polarization (P_m) and leakage current (mA)for each Dy^{3+} doped of SrBi $_{(2-x)}Dy_xNb_2O_9$ (SBN)ceramics: (a) undoped (x = 0.00), (b) x = 0.02, (c) x = 0.04 and (d) x = 0.06.*

3.8 Dielectric Study

Dielectric study is a prominent characterization technique for ferroelectric materials. It provides information on material inter-dipole interaction with the applied external field at different temperatures and frequencies.

In this study of Dy^{3+} doped SrBi $_{(2-x)}Dy_xNb_2O_9$ compositions (x = 0.00,0.02,0.04,0.06), frequency-independent behaviour is observed at room temperature during the observations of SBN ceramic. The dielectric constant observed from the plot of dielectric constant (ε) and frequency (Hz) for pure SBN (x=0.00) is 159.94. The introduction of Dy^{3+} ion (x=0.02) shows a slight decrease in dielectric constant to 156.74. Further increasing the concentration of Dy^{3+} ion (x=0.04) results in an increase in the dielectric constant to 219.59. Beyond x=0.04, a decrease in the value of the dielectric constant to 180.56 is observed. x=0.04 is the optimal doping of the Dy^{3+} ion in SBN ceramics. The recorded decrease beyond x=0.04 is attributed to lattice strain [24], resulting in reduced ferroelectric behaviour.

A straight line in the plot of dielectric constant (ε) and frequency(Hz)confirms excellent dielectric response with frequency, confirming that the given SBN ceramic is a highly ferroelectric material. Among all compositions, x=0.04 composition is the best fit for high-frequency electronic devices and energy storage applications such as capacitors and sensors [32,33,34,35].

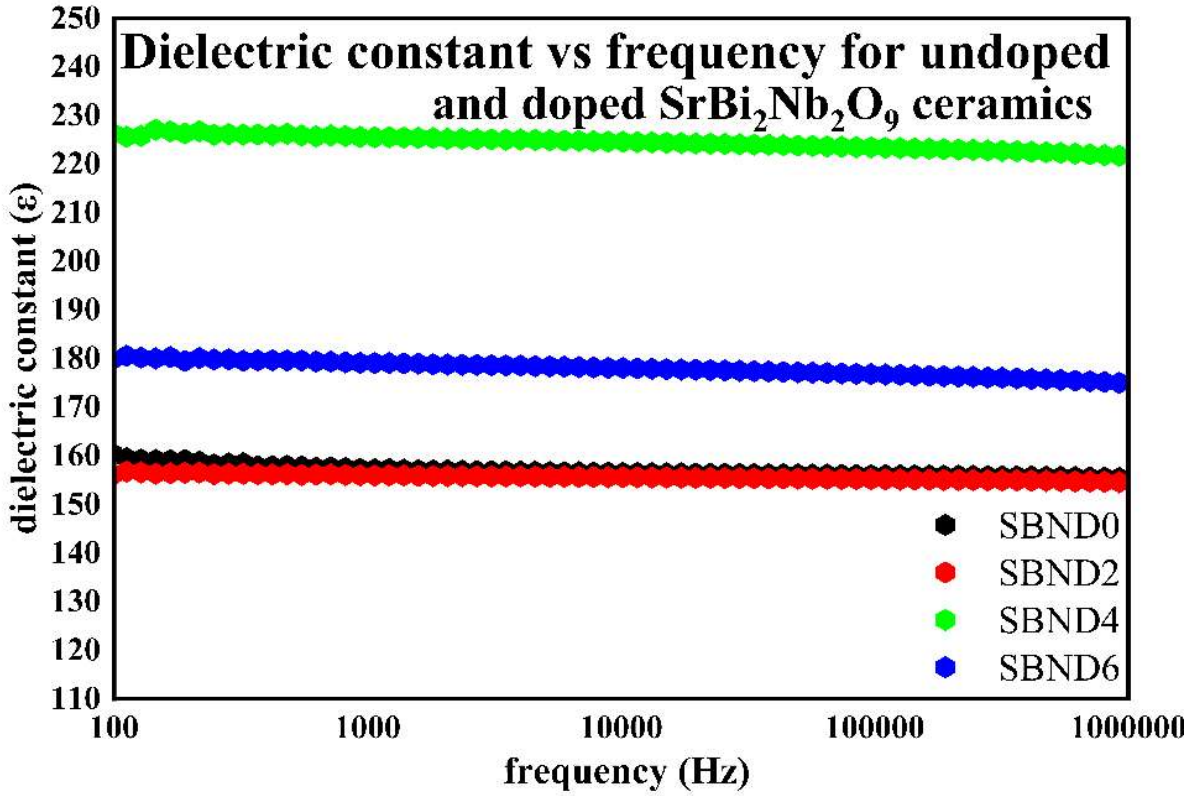

***Figure 11**: Frequency dependence of dielectric constant (ε) for different compositions of* $SrBi_{(2-x)}Dy_xNb_2O_9$*) where x=0,0.02,0.04,0.06.*

3.9 Photoluminescence (PL)

Photoluminescence is an optical characterization technique in which a material absorbs photons of a specific wavelength to emit lower-energy photons of longer wavelengths. In this process, electrons absorb energy to move to their higher energy states and relax back to lower energy states, resulting in characteristic luminescence.

In this study, PL spectra of Dy^{3+} doped $SrBi_{(2-x)}Dy_xNb_2O_9$ (x=0.00, 0.02, 0.04, 0.06) ceramics were recorded under UV excitation at 387nm[36].

The peak of Dy^{3+} ions was observed in the region of 480-490 nm, and, according to previous research, it corresponds to the characteristic blue emission of Dy^{3+} ions, arising from the $^4F_{9/2} \rightarrow {}^6H_{15/2}$ transition due to magnetic dipole interaction in the Dy^{3+} doped SBN ceramic [37,38].

The peak was observed in the region 575-580 nm, corresponding to the $^4F_{9/2} \rightarrow {}^6H_{13/2}$ transition known as Hypersensitive yellow emission, attributed to the electric dipole interaction inside the SBN ceramic [39].

The peak around 660nm is expected, but it is not visible due to its lower intensity as compared to the blue and yellow emissions. The transition corresponds to the $^4F_{9/2} \rightarrow {}^6H_{11/2}$ of the Dy^{3+} ion. It is characteristic of the metal oxide ceramic [40]. It is known as red emission.

Based on these observations, it is concluded that the Dy^{3+} doped metal oxide ceramics are suitable candidates for the production of white LEDs[37,38,41,42].

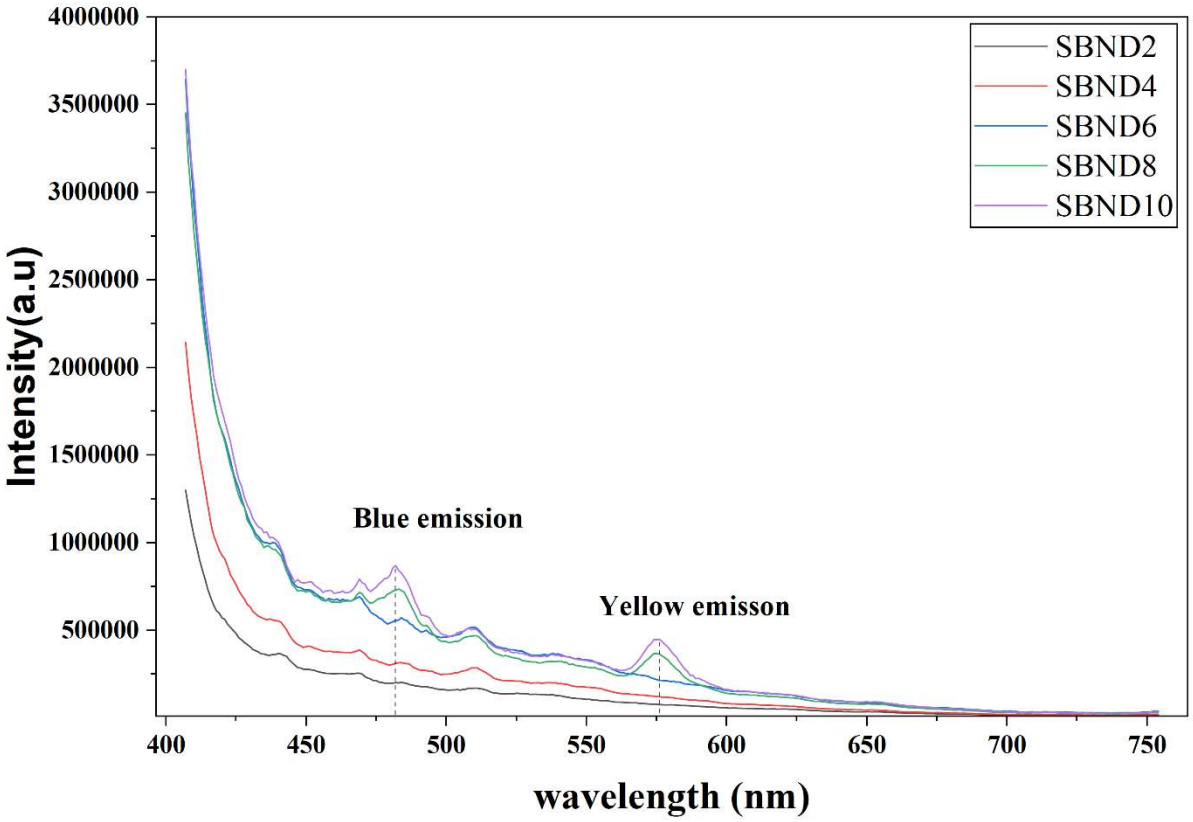

Figure 12: *PL spectra for different compositions of* $SrBi_{(2-x)}Dy_xNb_2O_9$ *(SBN) where* $x=0,0.02,0.04,0.06,0.08,0.10$.

CHAPTER-4

CONCLUSION

In this study, the successful incorporation of Dy^{3+} ion in the $SrBi_2Nb_2O_9$ lattice with the X-ray diffraction patterns (XRD) is confirmed. The materials were synthesized using the solid-state reaction (SSR) method. The diffraction patterns indicate the single-phase structure with no extra or secondary peaks, although a slight peak shift was observed with the increasing content of Dy^{3+} ion. The shift suggests minor distortion due to the difference between the ionic radius of Dy^{3+} and the Bi^{3+} ion. SEM images revealed a plate-like grain morphology, characteristic of layered perovskite systems, with uniform distribution across all doped samples. FTIR analysis indicates a high-quality ceramic with well-defined NbO_6 vibrational modes. PE hysteresis loop at room temperature reveals strong ferroelectric behaviour. The remanent polarization (P_r) increased with Dy concentration, showing improved ferroelectric switching. The temperature-dependent PE loop reveals that as the temperature increases, dipoles within the crystal lattice undergo more favourable alignment than at room temperature, owing to thermally activated wall domain motion. The fatigue analysis of the P-E loop reveals that it can retain its memory after a huge number of cycles of bipolar applied fields. The leakage current also reveals the same. Dielectric studies further confirmed frequency-independent dielectric behaviour with low dielectric loss, demonstrating that Dy doping improves energy efficiency. The study of PL Spectra reveals its application in the production of white LED_S. Hence, Dy^{3+} doped $SrBi_{(2-x)}Dy_xNb_2O_9$ (x=0.02,0.04,0.06) ceramics exhibited enhanced structural stability, ferroelectric, and dielectric properties, indicating their potential for high-frequency electronic and energy storage applications.

CHAPTER-5

APPLICATION AND FUTURE SCOPE

5.1 APPLICATIONS

Dy^{3+} doped $SrBi_{(2-x)}Dy_xNb_2O_9$ (SBN) belongs to the family of Aurivillius ferroelectric ceramics, which are widely recognized for their excellent electrical stability, low dielectric loss, high Curie temperature, and strong ferroelectric behaviour. Because of these characteristics, SBN and its modified forms hold significant potential for a wide range of advanced electronic applications.

One of the primary applications of Dy-doped SBN ceramics is in non-volatile ferroelectric random-access memory (FeRAM). The stable remnant polarization and low fatigue behaviour make these materials suitable for memory devices that require fast switching, low power consumption, and long data retention. Dy^{3+} doping enhances the structural stability and reduces defects, which helps improve the overall endurance of such memory elements. Another important area is high-frequency capacitors and dielectric components, where the dielectric constant and low dielectric loss play a crucial role. The improved dielectric performance observed in the Dy-substituted samples suggests their suitability for filters, resonators, and energy-storage capacitors in modern electronics. Additionally, Dy-modified SBN can be explored for energy-storage applications, where high breakdown strength and stable polarization behaviour are essential. The optimized composition (x = 0.04) shows improved ferroelectric loop characteristics that are beneficial for such devices. Overall, the enhanced electrical behavior of Dy^{3+} doped $SrBi_{(2-x)}Dy_xNb_2O_9$ (SBN) demonstrates that it is a strong candidate for next-generation electronic, electromechanical, and energy-storage applications.

5.2 FUTURE SCOPE

The study on Dy^{3+} doped $SrBi_{(2-x)}Dy_xNb_2O_9$ (x=0.00, 0.02, 0.04, 0.06) provides several promising directions for future research, particularly because Aurivillius ceramics continue to attract attention for advanced electronic and multifunctional applications. One potential area lies in optimizing dopant concentration beyond the limited range studied here. Since the 4% Dy^{3+} composition displayed the most favourable ferroelectric and morphological characteristics, it would be valuable to investigate finer doping steps around this concentration to identify the exact optimum level. Future studies can also focus on understanding the conduction mechanisms in these

materials using impedance spectroscopy, and temperature-dependent dielectric studies. These techniques can give clearer insights into how Dy^{3+} influences charge transport, domain wall motion, and relaxation processes within the SBN lattice. Additionally, the incorporation of co-dopants such as rare-earth ions (La^{3+}, Nd^{3+}, Gd^{3+}) may further tailor grain growth behaviour, reduce defects, and enhance energy-storage capability. Overall, the present study lays a strong foundation, and by extending it across new compositions, techniques, and device geometries, Dy-doped SBN ceramics hold immense potential for next-generation electronic and energy-storage technologies.

References

[1] Aurivillius, B. (1949). Mixed Bismuth Oxides with Layer Lattices. I. The Structure Type of $CaNb_2Bi_2O_9$. *Arkiv för Kemi*, 1, 463-480.

[2] Dhak, D., Biswas, S.K., & Pramanik, P. (2006). Synthesis and characterization of nanocrystalline $SrBi_2Nb_2O_9$ ferroelectric ceramics using TEA as the polymeric matrix. *Journal of the European Ceramic Society*, 26(16), 3717-3723. https://doi.org/10.1016/j.jeurceramsoc.2005.12.002

[3] Said, M., Velayutham, T.S., Gan, W.C., & Abd Majid, W.H. (2015). The structural and electrical properties of $Sr_xBa_{(1-x)}Nb_2O_6$ (SBN) ceramic with varied composition. *Ceramics International*, 41(5B), 7119-7124 https://doi.org/10.1016/j.ceramint.2015.02.023

[4] Amsei Júnior, N.L., Simões, A.Z., Cavalheiro, A.A., Zanetti, S.M., Longo, E., & Varela, J.A. (2008). Structural and microstructural characterization of $SrBi_2(Ta_{0.5}Nb_{0.48}W_{0.02})_2O_9$ powders. *Journal of Alloys and Compounds*, 454(1-2), 61-65. https://doi.org/10.1016/j.jallcom.2006.11.194

[5] Abdul Basith, Shobhangna Singh, Ankita Banwal, Megha Narwan, Manoj Verma, Renuka Bokolia, Regulating novel tunable green to red upconversion luminescence in Er3+/Yb3+ co-doped SrBi2Nb2O9 ferroelectric ceramic, Ceramics International, Volume 50, Issue 24, Part A,2024,Pages 52344-52355, ISSN 0272-8842, https://doi.org/10.1016/j.ceramint.2024.10.086.

[6] Cheng, S., Zhang, B., Ai, S., Yu, H., Wang, X., Yang, J., Zhou, C., Zhao, J., & Rao, G. (2023). Enhanced piezoelectric properties and thermal stability of $Bi_{0.5}Na_{0.5}TiO_3$ modified $BiFeO_3BaTiO_3$ ceramics with morphotropic phase boundary. *Journal of Materiomics*, 9(3), 464-471. https://doi.org/10.1016/j.jmat.2023.01.001

[7] Narwan, M., Banwal, A., Kumar, B., Verma, M., Shandilya, A., Rai, V. K., Sharma, R., & Bokolia, R. (2025). Ho^{3+}- driven novel orange emission and enhanced energy storage in lead-free $Bi_{0.5}Na_{0.5}TiO_3$ ceramics. *Ceramics International*, *51*(26), 48110-48121. https://doi.org/10.1016/j.ceramint.2025.08.070

[8] Indurkar, A., Mev, S. K., Asthana, S., & Subohi, O. (2025). Influence of $SrBi_2Nb_2O_9$ (SBN) incorporation in $K_{0.5}Na_{0.5}NbO_3$ (KNN) ceramics on its structural and electrical properties. *Physica B: Condensed Matter*, 706, 417144. https://doi.org/10.1016/j.physb.2025.417144

[9] Namsar, O., Watcharapasorn, A., & Jiansirisomboon, S. (2013). Phase, microstructure and ferroelectric properties of new complex-structured ferroelectric ceramics in the PZT–SBN system. *CeramicsInternational*, *39*(Supplement1),S103-S106. https://doi.org/10.1016/j.ceramint.2012.10.049

[10] Mohanty, R., Kaja, K. R., Hajra, S., Behera, S. A., Panigrahi, B. K., Kim, H. J., & Achary, P. G. R. (2026). EVA-$SrBi_2Nb_2O_9$ composites for energy harvesting and AI-integrated finger strength monitoring. *Materials Letters*, *410*, 140258.https://doi.org/10.1016/j.matlet.2026.140258

[11] Sankar, R., & Barbar, S. K. (2026). Exploration of the impact of rare earth elements (Nd, Sm, Gd, and Dy) doping on promising properties of Co_2SiO_4 ceramics for their use in power electronic modules and luminescent devices. *Journal of Alloys and Compounds*, *1051*, 186028. https://doi.org/10.1016/j.jallcom.2026.186028

[12] Song, X., Guo, S., Xu, Y., Lin, C., & Liu, X. (2026). Enhanced 2.9 μm emission in Dy^{3+}/Yb^{3+} co-doped fluorosilicate glass ceramics with KY_3F_{10} nanocrystals. *Journal of Non-Crystalline Solids*, *682*, 124083. https://doi.org/10.1016/j.jnoncrysol.2026.124083

[13] Pritam, A. (2024). Polaron assisted hopping mechanism in microwave processed Nd doped second layered aurivillius $SrBi_2Nb_2O_9$ ceramics. *Ceramics International*, 50(22), 48343-48353. https://doi.org/10.1016/j.ceramint.2024.09.184

[14] Mojumdar, P., Shaily, R., & Bokolia, R. (2021). Structural properties of Strontium Bismuth Niobate ($SrBi_2Nb_2O_9$) ferroelectric ceramics. *Materials Today: Proceedings*, 47(14), 4661-4665. https://doi.org/10.1016/j.matpr.2021.05.522

[15] Shaily, R., & Bokolia, R. (2021). Structural and photoluminescence properties of Er^{3+} doped $SrBi_2Nb_2O_9$ ceramics. *Materials Today: Proceedings*, 47(14), 4657-4660. https://doi.org/10.1016/j.matpr.2021.05.520

[16] Afqir, M., Tachafine, A., Fasquelle, D., Elaatmani, M., Carru, J.-C., Zegzouti, A., & Daoud, M. (2018). Synthesis and characterizations of Ho_2O_3 modified $SrBi_2Nb_2O_9$ ceramics. *Chinese Journal of Physics*, 56(3), 1158-1165. https://doi.org/10.1016/j.cjph.2018.04.018

[17] Xiao, J., Zhang, H., Xue, Y., Lu, Z., Chen, X., Su, P., Yang, F., & Zeng, X. (2015). The influence of Ni-doping concentration on multiferroic behaviors in $Bi_4NdTi_3FeO_{15}$ ceramics. *Ceramics International*, 41(1B), 1087-1092. https://doi.org/10.1016/j.ceramint.2014.09.033

[18] Garlapati, V. L., Jaladi, N. K., & Sangula, N. (2024). Exploring the multifunctional aspects of $SrBi_{2-X}(CoFe_2O_4)_XNb_2O_9$ nanocomposite materials emphasizing the structural, elastic, and optical properties. *Ceramics International*, 50(23), 49652-49666. https://doi.org/10.1016/j.ceramint.2024.09.310

[19] Anasser, I., Harech, M. A., Labbilta, T., Barbouchi, A., Afqir, M., Hadouch, Y., Lakouader, A., Mezzane, D., Zegzouti, A., & Daoud, M. (2025). Enhancing $SrBi_2Nb_2O_9$ ceramics: The role of neodymium substitution in structural, dielectric, and ferroelectric properties. *Ceramics International*, *51*(1), 1204-1213. https://doi.org/10.1016/j.ceramint.2024.11.101

[20] Ahn, Y., & Son, J. Y. (2025). High-performance energy storage in La-modified $Sr_{0.5}Ba_{0.5}Nb_2O_6$ thin films with tetragonal tungsten bronze structure. *Ceramics International*, *51*(29B), 61305-61314. https://doi.org/10.1016/j.ceramint.2025.10.325

[21] Song, J.Y., Zhao, B.C., Huang, Y.N., Qin, Y.F., Zhu, X.B., Song, W.H., & Sun, Y.P. (2016). Structure, magnetic, electrical and thermal transport properties of Dy-doped $Ca_3Co_2O_6$ ceramics. *Ceramics International*, 42(7), 8955-8961. https://doi.org/10.1016/j.ceramint.2016.02.154

[22] Satyarthi, S. K., Singh, V. P., Singh, C. B., Kumar, D., & Singh, A. K. (2025). Band gap engineering and multicolor emission in environment friendly Dy-Ti Co-doped $LiNbO_3$ ceramics for advanced electrical energy storage, LED and laser applications. *Ceramics International*, *51*(19), 28058-28072. https://doi.org/10.1016/j.ceramint.2025.04.021

[23] Zou, H., Yu, Y., Li, J., Cao, Q., Wang, X., & Hou, J. (2015). Enhancement of dielectric and ferroelectric properties of dysprosium substituted $SrBi_2Ta_2O_9$ ceramics. *Journal of Materials Science: Materials in Electronics*, *26*(12), 9814–9821. https://doi.org/10.1007/s10854-015-3930-2

[24] Huang, C. J., Liu, Y., & Pennycook, S. J. (2015). Variation of ferroelectric hysteresis loop with temperature in $(Sr_xBa_{1-x})Nb_2O_6$ unfilled tungsten bronze ceramics. *Journal of Materials Research and Technology*, *4*(2), 1–8. https://doi.org/10.1016/j.jmrt.2015.03.003

[25] Yang, J., Song, D.P., Yin, Y., Chen, L.Z., Chen, L.-Y., Wang, Y., & Wang, J.Y. (2019). Ferroelectric polarization and fatigue characterization in bismuth-based Aurivillius thin films at lower voltage. *Materials Science and Engineering: B*, *248*, 114408. https://doi.org/10.1016/j.mseb.2019.114408

[26] Paz de Araujo, C. A., Cuchiaro, J. D., McMillan, L. D., Scott, M. C., & Scott, J. F. (1995). Fatigue-free ferroelectric capacitors with platinum electrodes. *Nature*, *374*(6523), 627–629. https://doi.org/10.1038/374627a0

[27] Rojac, T., Kosec, M., Budic, B., Setter, N., & Damjanovic, D. (2012). Mechanism of polarization fatigue in $BiFeO_3$. *ACS Nano*, *6*(10), 8862–8871. https://doi.org/10.1021/nn303090k

[28] Peláiz-Barranco, A., & Guerra, J. D. S. (2015). Polarization and thermally stimulated processes in lead-free ferroelectric ceramics. In *Lead-Free Ferroelectrics*. IntechOpen. https://doi.org/10.5772/60672

[29] Joo, H. W., & Lee, H. Y. (2002). Leakage current and fatigue in ceramic ferroelectric oxides. *Key Engineering Materials*, *206–213*, 1309–1312. https://doi.org/10.4028/www.scientific.net/KEM.206-213.1309

[30] Silva, M. S., Zabotto, F. L., & Garcia, D. (2024). Fatigue endurance and leakage characteristics of ferroelectric $BaBiO_3$ thin films obtained by the polymeric precursor method. *Journal of Alloys and Compounds*, *1010*, 177456. https://doi.org/10.1016/j.jallcom.2024.177456

[31] Genenko, Y. A., Glaum, J., Hoffmann, M. J., & Albe, K. (2015). Mechanisms of aging and fatigue in ferroelectrics. *Materials Science and Engineering B*, *192*, 52–82. https://doi.org/10.1016/j.mseb.2014.10.003

[32] Erdogan, E., Kocyigit, A., & Yilmaz, M. (2026). Electrical characterization of Cr-doped $ZnZrTa_2O_8$ microwave ceramics: Effects of temperature and frequency. *Ceramics International*. https://doi.org/10.1016/j.ceramint.2026.03.281

[33] Shi, J., Dong, R., He, J., Wu, D., Tian, W., & Liu, X. (2023). Regulating ferroelectric polarization and dielectric properties of BT-based lead-free ceramics. *Journal of Alloys and Compounds*, *933*, 167746. https://doi.org/10.1016/j.jallcom.2022.167746

[34] Mohammad, M. M. (2025). Structure, morphological, frequency-dependent electrical and enhanced dielectric properties of multilayers ceramic prepared from Sr-doped $BaTiO_3$. *Materials Technology*, *40*(1). https://doi.org/10.1080/10667857.2025.2563216

[35] Xu, D., Zhao, W., Cao, W., Li, W., & Fei, W. (2021). Electrical properties of Li and Nb modified $BiFeO_3$ ceramics with reduced leakage current. *Ceramics International*, 47(3), 4217-4225. https://doi.org/10.1016/j.ceramint.2020.09.300

[36] Singh, R., Luthra, V., Rawat, R.S., & Tandon, R.P. (2015). Enhancement of dielectric and ferroelectric properties of dysprosium substituted $SrBi_2Ta_2O_9$ ceramics. *Journal of Materials Science: Materials in Electronics*, 27, 1977–1987. https://doi.org/10.1007/s10854-015-3930-2

[37] Ankoji, P., Suresh Kumar, N., Chandra Babu Naidu, K., & Pradeep Raju, B. (2021). Structural and luminescence properties of Dy^{3+}-doped $La_2(MoO_4)_3$ phosphors. *Applied Physics A*, *127*(7), 552. https://doi.org/10.1007/s00339-021-04709-0

[38] Wang, X., Li, X., Xu, S., Cheng, L., Sun, J., Zhang, J., Zhang, X., & Chen, B. (2020). Luminescence properties of color-tunable YNbO4: Dy^{3+}, Tm^{3+} phosphors. Journal of Asian Ceramic Societies, 8(4), 1076–1083. https://doi.org/10.1080/21870764.2020.1815347

[39] Yawale, P. R., Mungmode, C. D., Gahane, D. H., & Mohurley, I. S. (2024). Blue-yellow emitting Dy^{3+} doped $K_2Y_2B_2O_7$ novel phosphor for WLED application. Journal of Optics, 53(7), 801–808. https://doi.org/10.1007/s12596-023-01400-w

[40] Ramachandran, R., Kadam, A. R., & Sreeramulu, B. (2022). Comprehensive spectroscopic investigations and yellow emission capabilities of Dy^{3+} activated novel phosphors for lighting applications. Journal of Luminescence, 241, 118485. https://doi.org/10.1016/j.jlumin.2021.118485

[41] Salerno, E. V., Eliseeva, S. V., Petoud, S., & Pecoraro, V. L. (2024). Tuning white light emission using single-component tetrachroic Dy^{3+} metallacrowns: the role of chromophoric building blocks. Chemical Science, 15(21), 8012–8024. https://doi.org/10.1039/D4SC00389F

[42] Reddy, L. (2023). A Review of the Efficiency of White Light (or Other) Emissions in Singly and Co-Doped Dy3+ Ions in Different Host (Phosphate, Silicate, Aluminate) Materials. Journal of Fluorescence, 33(6), 2181–2192. https://doi.org/10.1007/s10895-023-03250-y

CHAPTER-6

Appendix

Conference Record

Proof of Registration

IAMSSG Secretary <secretary.iamssg@jecrcu.edu.in> Fri, 17 Oct 2025, 14:37
to bcc: me

Dear Participant,

Greetings from the Organizing Committee of **IAMSSG 2025**!

We are pleased to confirm your participation in the ***International Conference on Innovations and Advances in Material Science for Sustainable Goals (IAMSSG 2025)***, scheduled to be held from **October 29–31, 2025**, at **JECRC University, Jaipur**.

Kindly note the following important instructions:

1. For prompt and easy communication, you are requested to join the official WhatsApp group using the link below:
   🔗 Join WhatsApp Group
2. Session details and updates will be shared through this group.
3. Information regarding the **oral/poster presentation schedule** will also be updated there.

For any queries, feel free to contact us at 📧 **secretary.iamssg@jecrcu.edu.in**.

Payment Receipt

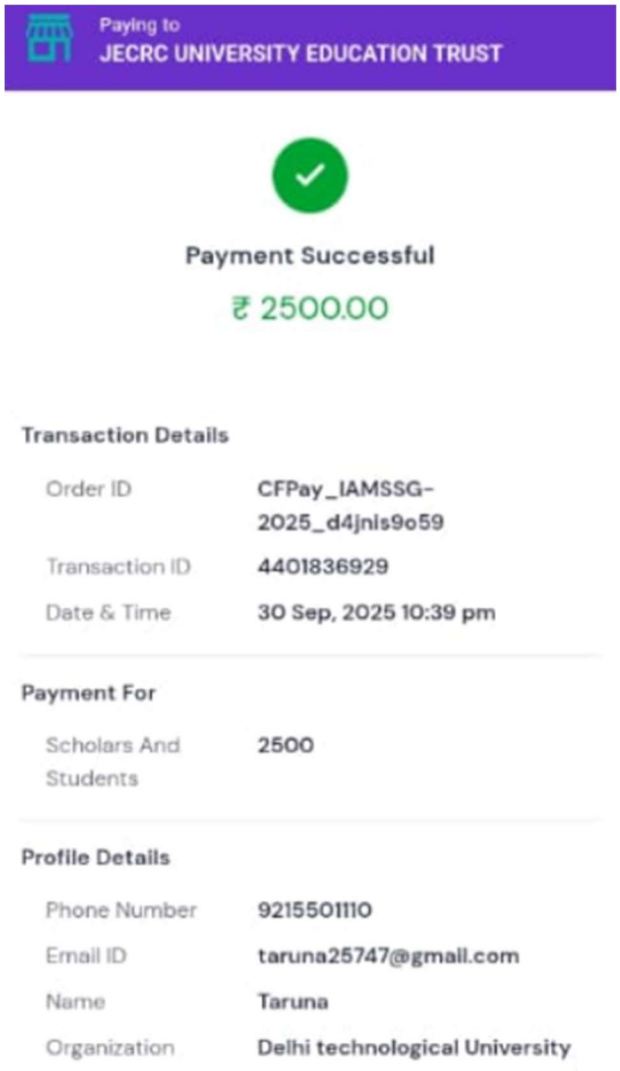

Poster Presented

turnitin Page 55 of 59 - Integrity Submission Submission ID trn:oid:::3618:140679551

IAMSSG, 2025

Study of Electrical Properties of Dy^{3+} doped $SrBi_2Nb_2O_9$ aurivillius ceramic for advanced electronic applications

Taruna, Divyansh Ranjan Varshney, Surya Pratap Singh, Megha Narwan, Renuka Bokolia*

Email:taruna25747@gmail.com, divya2kranjan@gmail.com, renukabokolia@dtu.ac.in*

FMRL, Department of Applied Physics, Delhi Technological University, Delhi-110042, India

IAMSSG-P-32

ABSTRACT

A series of ferroelectric ceramics with the composition $SrBi_{(2-x)}Dy_xNb_2O_9$ (SBN) were synthesized using the conventional solid state reaction method. X-ray diffraction (XRD) confirmed the formation of a single-phase orthorhombic structure, indicating successful incorporation of Dy^{3+} ions into the lattice. The substitution of Dy^{3+} caused systematic variations in lattice parameters and unit cell volume, suggesting localized structural distortion. Scanning electron microscopy (SEM) revealed a plate-like grain morphology with random orientation, characteristic of layered perovskite systems. Dielectric studies shows well-defined ferroelectric characteristics with low dielectric loss, while PE hysteresis measurements confirmed the ferroelectric behaviour of all compositions. The variation in remanent polarization (P_r) and coercive field (E_c) with Dy content indicates that dopant concentration significantly influences ferroelectric switching characteristics. Overall, Dy^{3+} substitution in SBN ceramics enhances structural stability and dielectric performance, making these materials promising candidates for high-frequency electronic devices and energy storage applications.

Introduction

- This study focuses on developing scientific understanding of single-phase Aurivillius-type $SrBi_2Nb_2O_9$ (SBN) ceramics doped with Dy^{3+} ions.
- It belongs to the Bismuth Layered Structure Ferroelectrics (BLSF) family, known for its unique layered perovskite-like structure, which can be improved by doping with rare-earth elements like Dy^{3+}, Nd^{3+}, and Er^{3+}.
- In this work, Dy^{3+} -doped $SrBi_{2-x}Dy_xNb_2O_9$ (x = 0.02, 0.04, 0.06) ceramics were synthesized and analyzed to examine how Dy^{3+} substitution affects their structural and electrical properties.

Methodology

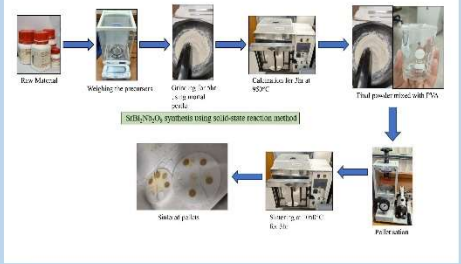

Results and Discussions

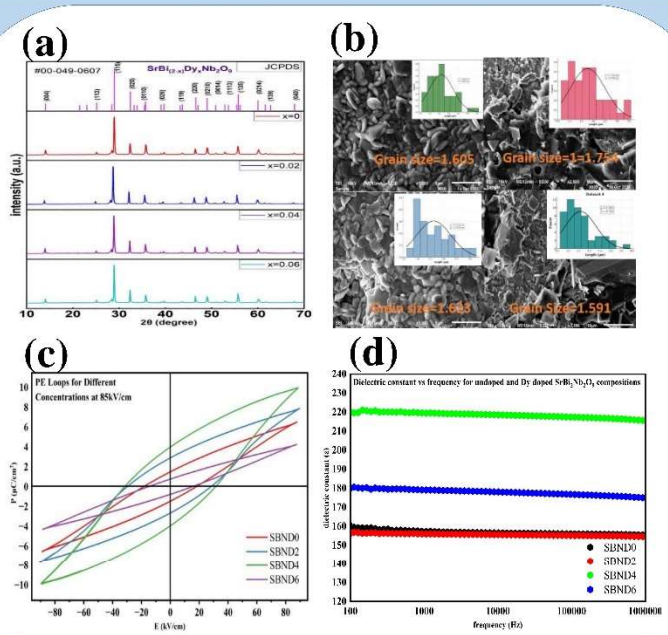

Fig.:-(a) XRD spectra (b) SEM images (c) PE Loops (d) Dielectric spectra of undoped and Dy doped SBN.

Conclusion

- The formation of a single-phase Aurivillius-type orthorhombic structure and the successful incorporation of Dy ions into the SBN lattice is confirmed from the XRD Spectra.
- The average grain size is calculated from the SEM microstructures of all the undoped and doped SBN compositions.
- The samples exhibited significant remanent polarisation (Pr) values for increasing Dy^{3+} concentrations.
- The frequency-independent Dielectric spectra confirm the ferroelectric characteristics of the prepared SBN compositions.

References

[1] Abdul Basith, Shobhangna Singh, Ankita Banwal, Megha Narwan, Manoj Verma, Renuka Bokolia, "Regulating novel tunable green to red upconversion luminescence in Er3+/Yb3+ co-doped SrBi2Nb2O9 ferroelectric ceramic", Ceramics International, Vol 50 (24), 2024, 52344-52355.
[2] Banwal, R. Bokolia, "Effect of Er3+ Ion Doping on Structural, Ferroelectric, and Up/down Conversion Luminescence in BaBi2Nb2O9 Ceramic, vol. 47, 2021, pp. 4692 4695, 03.

Acknowledgements

The authors are thankful to the Functional Material Research Laboratory (FMRL) and DTU for providing facilities to carry out the research work.

Participation Certificate

JECRC UNIVERSITY
BUILD YOUR WORLD

CELEBRATING 25 YEARS

JMCH
JECRC Medical College and Hospital

in association with

SMRS
SOFT MATERIALS RESEARCH SOCIETY
JAIPUR, INDIA

IAPT

International Conference
on
Innovations, Advances in Material Science for Sustainable Goals (IAMSSG 2025)

IAMSSG

October 29-31, 2025

Organized by : **Department of Physics, JECRC University, Jaipur, Rajasthan**
(Sponsored by **ANRF, DST - Rajasthan**)

CERTIFICATE OF PAPER/POSTER PRESENTATION

This is to certify that the paper/poster entitled Electrical and Optical study of Bi^{3+} doped--- advanced electronic applications authored by .....

has been presented by .....Tanuja.....

Prof. Pranav Saxena
Convener

Prof. Widhi Dubey
General Chair

Prof. Victor Gambhir
President, JECRC University

Award received


LANGMUIR
IAMSSG
ACS Publications
Most Trusted. Most Cited. Most Read.
RECOGNIZES
TARUNA
FOR BEST POSTER
IAMSSG 2025 : International Conference on
"Innovations, Advances in Material Science for Sustainable Goals"
JECRC University, Jaipur, India
October 29 – 31, 2025

turnitin Page 59 of 59 - Integrity Submission Submission ID trn:oid:::3618:140679551